AERO3410 – Group Assignment
Structural Analysis Project

Group R

Peleg Mondry Cohen z5476963

Shantanu Patil z5479486

Reece Nhan z5479091

Mehmet Furkan Yavuz z5481625

Gregory Papantoniou z5479578

Camille Lu z5676697

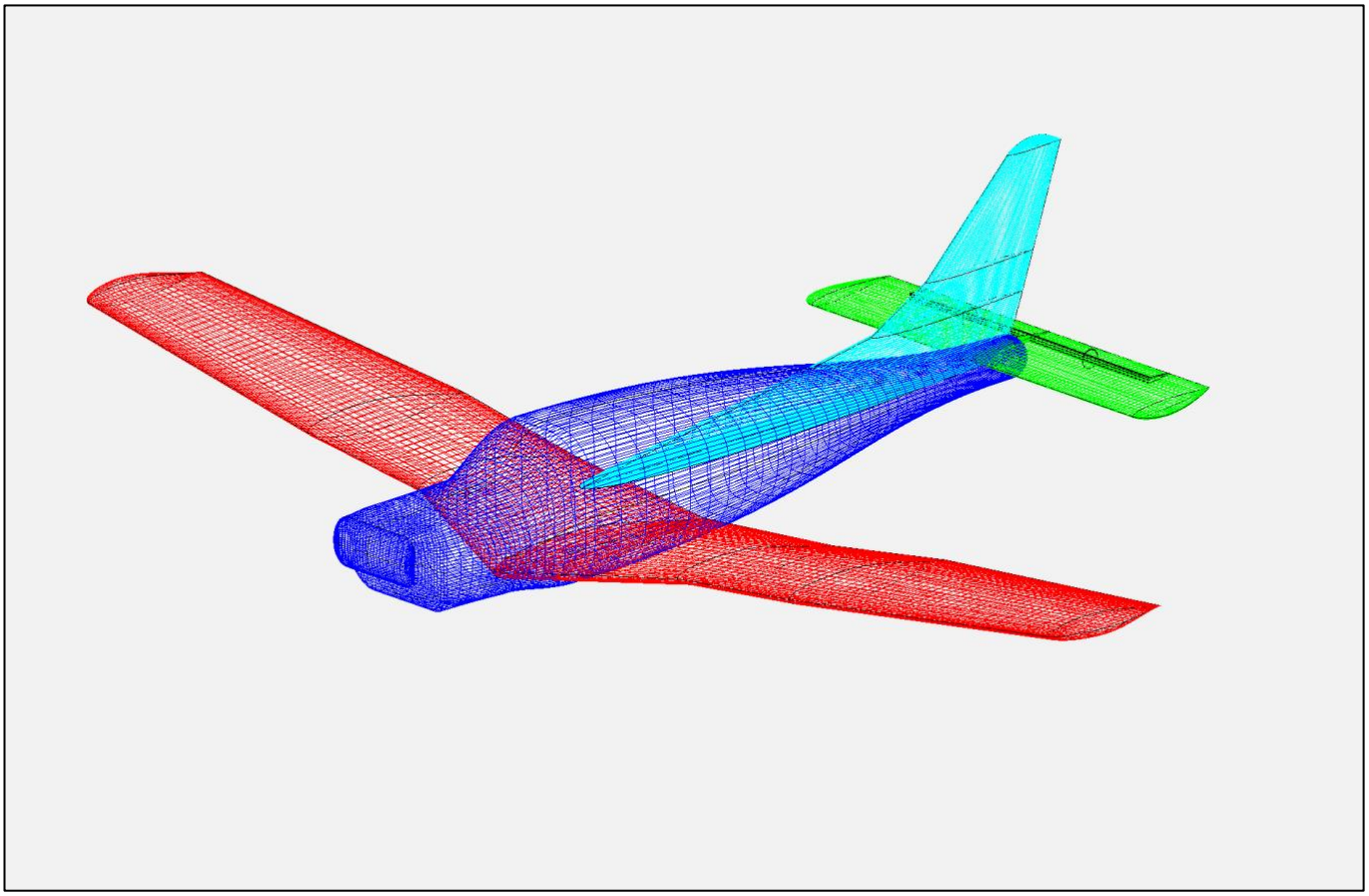

1 Executive Summary

The Piper Archer is a single-propellor driven aircraft commonly utilised in training scenarios. When correctly maintained, and flown, the structural components of the aircraft should not be affected by fatigue or failure and can be expected to operate almost indefinitely. This investigation aims to prove this claim by analysing the stresses on the fuselage and wings during landed, maximum climb and ultimate loading case. Unlike commercial airliners which can be expected to be completing a cyclic set of manoeuvres per flight, the Piper Archer II does not have a fixed use case and so, a range of simulation tools including OpenVSP, COMSOL and MATLAB were utilised to provide a snapshot of the forces, stresses, and eventual fatigue on the aircraft. Reasonable assumptions were made to simplify the aircraft's structure, using the manufacturer documentation where possible. A set of common training manoeuvres were produced to generalise the aircraft's durability and resilience to fatigue/failure.

The investigation finds that the Piper Archer is a sturdy aircraft that, when used correctly, remains under the endurance limit for fatigue and as such will continue to last almost indefinitely. In the presence of extreme stress concentrations, the component lifespan exists in the magnitude of 10^5 cycles. The investigation also found that with the geometry assumptions made, the fuselage would be well capable of withstanding a critical loading of 6.6G's. However, the wing experiences severe stiffener column buckling, the precursor to global buckling, which is a catastrophic failure mode. It is concluded that better wing geometry assumptions are required, as the assumptions for the panel length on the wings are far higher than in actuality due to a lack of available information; this induced a far lower initiating stress than likely, which resulted in the low margins of safety determined. This report should be taken as nothing more than a basis for the estimated lifespan of the Piper Archer II. Detailed analysis should be and can be completed with access to experimental data from flights, measuring real loads and stresses experienced by the aircraft components, enabling more accurate analysis.

Contents

Authors: z5476963, z5479486, 5479091, z5481625, z5479578, z5676697

Authors: z5476963, z5479486, 5479091, z5481625, z5479578, z5676697

2 Introduction and Aims

Aircraft structures must reliably withstand a combination of aerodynamic loads, inertial forces and operational stresses throughout its expected service life. Ensuring the structural integrity of the airframe is critical, not only for maintaining performance and complying with regulatory requirements, but also for occupant safety. This report aims to validate the structural integrity of the Piper Archer II by examining the expected loading the aircraft will experience throughout its lifetime and the safety margins associated with them.

The aircraft is analysed under three different load cases (section 3.3), landed on the ground, steady climb and under legally defined ultimate loading conditions. All of these originate from common mission profiles with the ultimate loading to account for a severe emergency such as pulling out of a dive.

For each load case, the critical shear forces and bending moments have been determined. Then, using a simplified model of the airframe, the corresponding critical stresses acting on the airframe have been calculated and analysed to ensure the aircraft will not fail or excessively fatigue throughout its expected service life.

The Piper Archer II is a popular general aviation aircraft that is primarily used for recreational flying, touring and training purposes. It was first certified in 1975 under the United States Federal Aviation Administration (FAA) type certificate data sheet no. 2A13.

General Specifications (Piper Aircraft Corporation, 1994):

- Maximum T/O weight: 2550 lb
- Empty Weight: 1416 lb
- Fuel Capacity: 48 gal
- Engine: Lycoming O-360-A4A or -A4M with 180 hp
- Never Exceed Speed: 148 knots (76 m/s)
- Max Climb Rate: 740 fpm
- Max Permissible Load Factor: 4.5

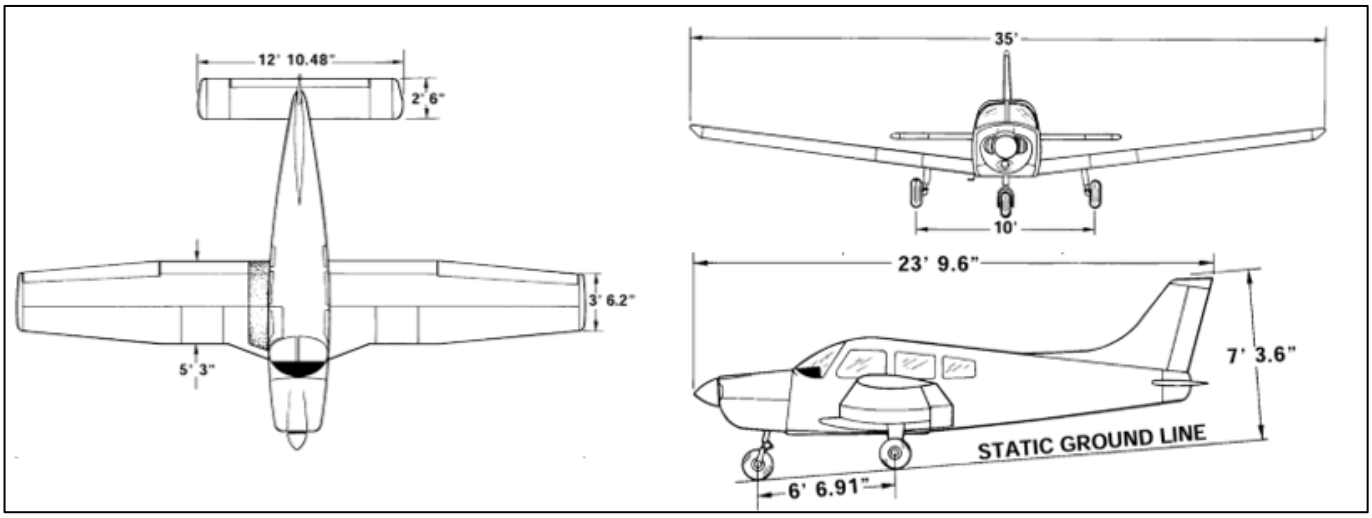

Figure 1: Three View – Archer II (Piper Aircraft Corporation, 1994)

This report utilises the standard direction convention used for aircraft analysis, as seen in *Figure 2Figure*

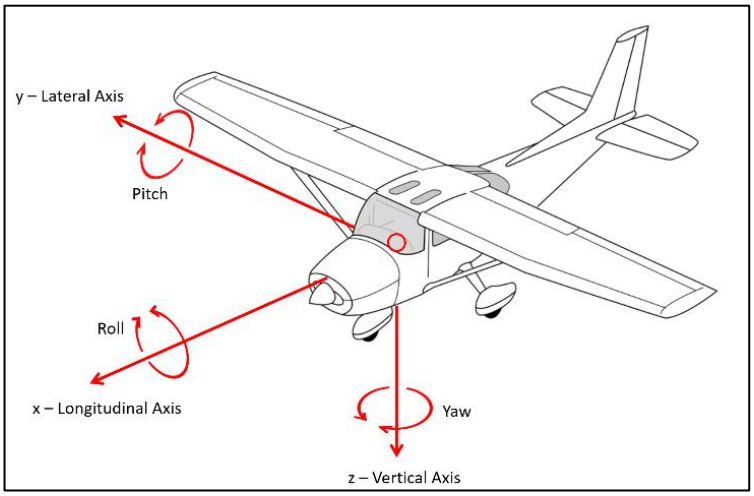

2: Analysis Direction Convention Used in this Report.

Figure 2: Analysis Direction Convention Used in this Report

3 Assumptions and Simplifications

The stress analysis for the Piper Archer II is complex and simplifications were made to reduce the task to a manageable level. With any approximation, assumptions reduce the accuracy of the end result, and so this section aims to outline some sources of error along with specifications of what simplifications were made.

3.1 Weight and Load Distribution over Wings

While there is no publicly available information on the self-weight of the wings of the Piper Archer II, a statistical analysis of existing designs reveals that the wings constitute about 17-27% of the aircraft empty weight, for general aviation aircraft (Al-Shamma & Ali, 2014). In order to use this statistic to the analysis of the aircraft in a valid manner, the lowest estimate should be used (17%). This is because as the weight of the wing acts in the opposite direction to lift, using a lower estimate for the wing weight would result in higher calculated forces and moments on the wings. As this report is concerned with the strength of the airframe and ensuring the design does not fail, it is best to use a conservative estimation.

An evenly distributed self-weight for the wing is assumed. As before, this is a conservative simplification as the wing tapers towards the end, meaning that the distributed self-weight of the wing decreases with distance from the fuselage, producing less bending moment. Fuel is assumed to be a point load, and the fuel tank is assumed to always be full during the analysis to maximise airframe loading.

3.2 Fuselage Weight and Simplified Geometry

3.3 There is no publicly available information on the self-weight of the fuselage, however, the fuselage weight can be assumed by subtracting the assumed self-weight of the wings (3.1 Weight and Load Distribution over Wings

While there is no publicly available information on the self-weight of the wings of the Piper Archer II, a statistical analysis of existing designs reveals that the wings constitute about 17-27% of the aircraft empty weight, for general aviation aircraft (Al-Shamma & Ali, 2014). In order to use this statistic to the analysis of the aircraft in a valid manner, the lowest estimate should be used (17%). This is because as the weight of the wing acts in the opposite direction to lift, using a lower estimate for the wing weight would result in higher calculated forces and moments on the wings. As this report is concerned with the strength of the airframe and ensuring the design does not fail, it is best to use a conservative estimation.

An evenly distributed self-weight for the wing is assumed. As before, this is a conservative simplification as the wing tapers towards the end, meaning that the distributed self-weight of the wing decreases with distance from the fuselage, producing less bending moment. Fuel is assumed to be a point load, and the fuel tank is assumed to always be full during the analysis to maximise airframe loading.

3.4 Fuselage Weight and Simplified Geometry
) from the basic empty weight of the entire aircraft.

Separate assumptions were made about the fuselage cross-sectional geometry for the calculation of aerodynamic loads (4.2 Fuselage Aerodynamic Loads and Centre of Pressure Determination) and for the fuselage stress analysis (6.3 Fuselage). These assumptions are detailed in each respective section.

3.5 Load Cases
<u>Load Scenario 1 – Maximum Climb</u>
This load scenario was chosen as it is a loading scenario the aircraft encounters on day-to-day operations and is based on the aircraft's maximum climb rate of $740 fpm$.
Parameters:

- Thrust: 3433 N
- Load Factor: 1
- Pitch: 15.45° Nose Up
- Roll: 0°
- Angle of Attack: 9.95°
- Velocity: 39 m/s

<u>Load Scenario 2 – Critical Loading</u>
This load scenario is defined as 1.5 times the maximum rated load factor and is the ultimate load the aircraft must withstand without failing. It was chosen as by analysing the airframe under this scenario and confirming it can withstand the involved loads, it ensures that the aircraft can safely handle all lower, non-critical loads. This also validates the published safety margin of 1.5 times the maximum load and ensures that it is appropriate for this aircraft.
Parameters:

- Thrust: 3064 N
- Load Factor: 6.6
- Pitch: 15.26° Nose Up
- Roll: 0°

- Angle of Attack: 15.26°
- Velocity: 76 m/s

Load Scenario 3 – Landed

This load scenario was chosen as it represents where the aircraft spends a significant portion of its working life – parked and stationary. It aims to act as a baseline that later results can then be compared to, while still being relevant to the lifecycle analysis of the aircraft.

Parameters:

- Thrust: 0 N
- Load Factor: 1
- Aircraft is stationary, on the ground and resting on its landing gear.

3.6 Material Properties

The airframe and skin of the Piper Archer II is known to be composed from a variety of Aluminium alloys. Figure 51-1 of the Piper PA-28-181 Aircraft Maintenance Manual (Piper Aircraft Corporation, 1994) shows that the most common material utilised is Al 2024-T3. This material is generally used in aerospace having been known for having excellent resistance to fatigue and a high strength-to-weight ratio. The material properties for Al2024-T3 are shown in Table 1.

Property	Imperial	Metric
Density	$0.1 lb/in^3$	$2780 kg/m^3$
Ultimate Tensile Strength	$70000 psi$	$483 MPa$
Tensile Yield Strength	$50000 psi$	$345 MPa$
Elastic Modulus	$10600 ksi$	$73.1 GPa$
Shear Modulus	$4060 ksi$	$28 GPa$
Poisson's ratio	0.33	0.33
Fatigue Strength	$20000 psi$	$138 MPa$
Fracture Toughness	$20000 psi$	$138 MPa$
Wing Skin thickness	$0.025 in$	$0.635 mm$

Table 1: Material Properties Al2024-T3

Throughout this report AL2024-T3 and the above material properties have been applied to all elements of the structural analysis.

4 Loading

4.1 Wings

Wing Geometry

To determine the loads acting on the wings during the three load cases, the geometry of the wings must first be considered.

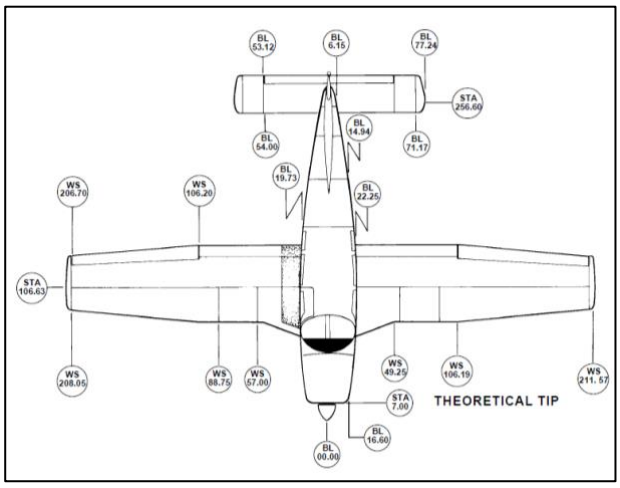

Figure 3: Aircraft Top View with Station References (Piper Aircraft Corporation, 1994)

As *Figure 3:* Aircraft Top View with Station References (Piper Aircraft Corporation, 1994) is to scale, it was possible to obtain other crucial dimensions for the wings of the aircraft, even ones that were not marked by station references. This was achieved by loading the drawing into a CAD program and then scaling it to its true size using the station references. Obtaining any missing dimensions was then achieved by drawing sketch lines in the program according to the drawing and measuring the length of

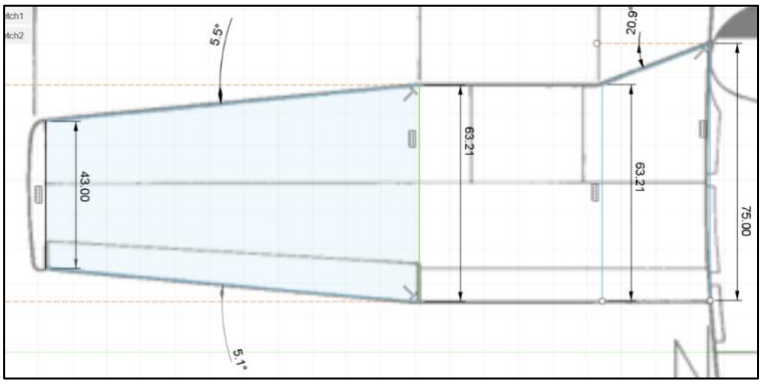

those lines.

Figure 4: An Example of Measuring Wing Geometry Using Scaled Drawings in CAD

To validate the measurements made using this technique, several additional measurements were made for locations marked by station references that were not used for the size calibration of the drawing.

Table 2 – Evaluation of CAD Measurements Accuracy

Measurement	Station Reference (inch)	CAD Measurement (inch)	%Error
Horizontal Distance to Wing Tip	211.57	213.12	0.73
Untapered Section Chord	63	63.21	0.33
Tip Chord	42.2	43	1.90
Horizontal Distance to Fuel Tank	57.00	57.37	0.65

As can be seen in Table 2 – Evaluation of CAD Measurements Accuracy, while there was some error present between the CAD measurements and then published measurements, that error tended to be very small, validating the use of this technique for further analysis in this report. The main source of error using this technique is that the limited resolution of the drawing added some ambiguity to where the measurements were taken (eyeballing the CAD sketch line placements according to the drawing).

Other key geometry features (skytamer.com, 1998)

- Wing Profile: NACA65(2)-415
- Dihedral 7°
- Incidence 2° at root, -1° at tip (gradual transition is assumed)

OpenVSP Analysis

OpenVSP is a parametric aircraft geometry tool that allows for the creation and analysis of 3D models that have been defined by engineering parameters. OpenVSP was developed for NASA and released as an open-source project. The software was used for the determination of the lift and drag distribution over the complex wing of the aircraft.

To perform the analysis, the wings were first modelled in OpenVSP using the geometry parameters previously outlined.

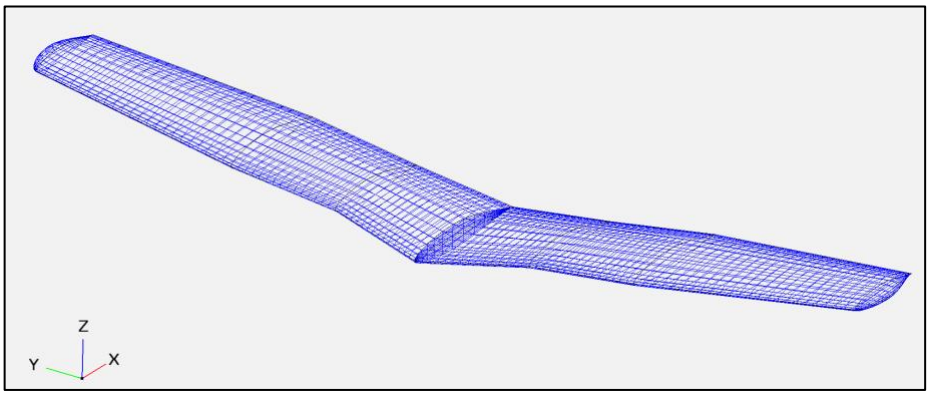

Figure 5: Wing Geometry in OpenVSP

After the geometry was modelled, VSPAERO, a potential flow aerodynamics tool that's integrated into OpenVSP was used to determine the lift and drag coefficient distributions over the wing for the different load scenarios. Using OpenVSP and VSPAERO to model and analyse the wing at the different load scenarios produces a more accurate load model than would be the case had a perfect elliptical lift distribution been assumed.

Scenario 1 – Maximum Climb

- Velocity: 39.1 m/s
- Angle of Attack: 9.95°
- Sea Level ($\rho_{air} = 1.225$ kg/m^3, $P = 101.35$ kPa, $c = 340.3$ m/s)

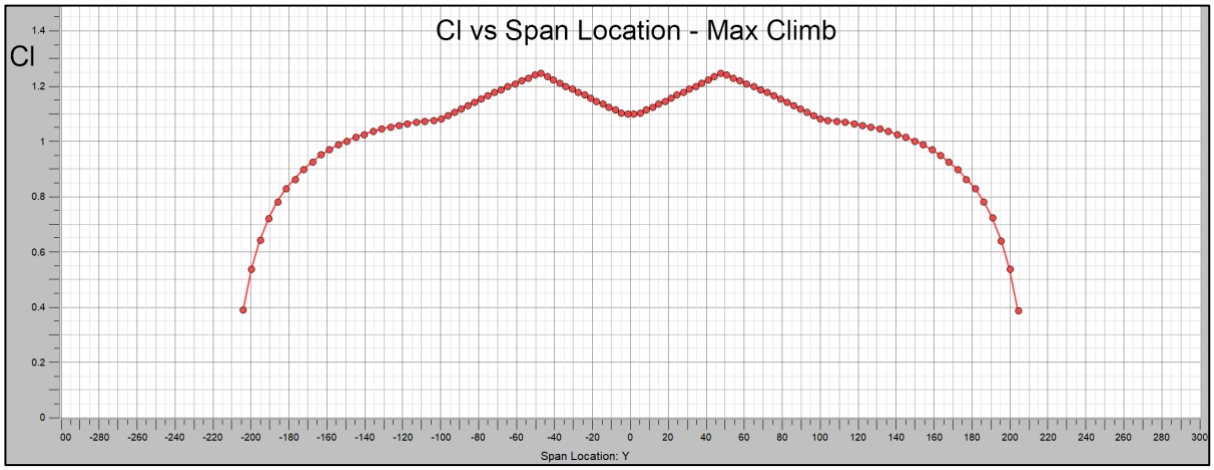

Figure 6: Lift Coefficient C_l vs Span Location – VSPAERO Result for Max Climb Scenario

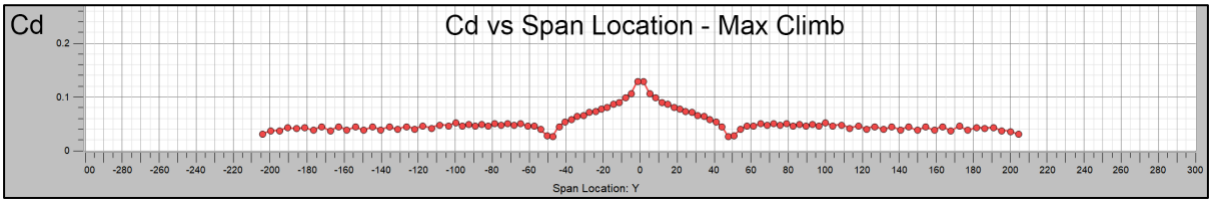

Figure 7: Drag Coefficient C_d vs Span Location – VSPAERO Result for Max Climb Scenario

Scenario 2 – Critical Loading

- Velocity: 76.4 m/s
- Angle of Attack: 15.26°
- Sea Level ($\rho_{air} = 1.225$ kg/m^3, $P = 101.35$ kPa, $c = 340.3$ m/s)

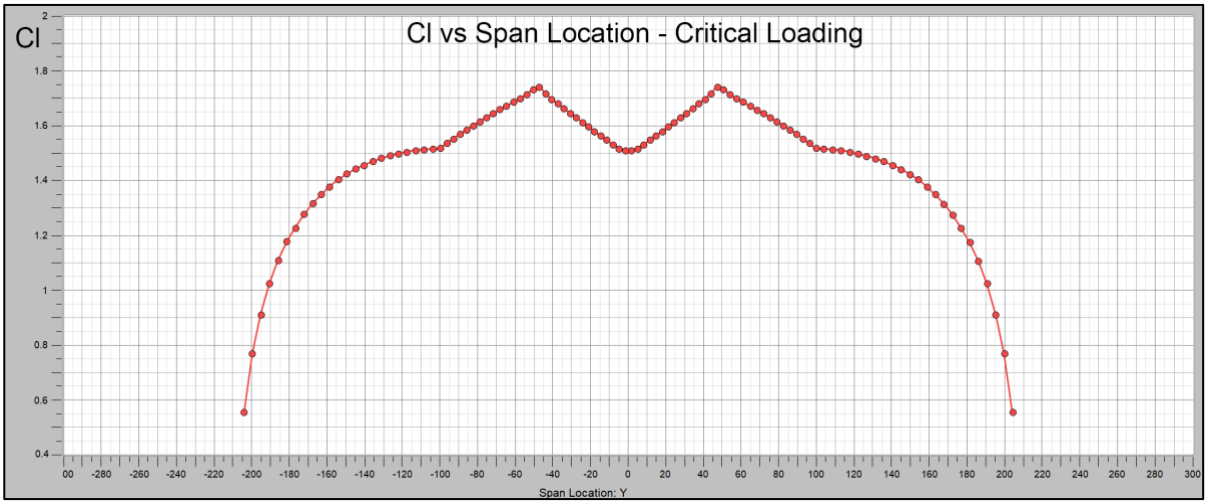

Figure 8: Lift Coefficient C_l vs Span Location – VSPAERO Result for Critical Loading Scenario

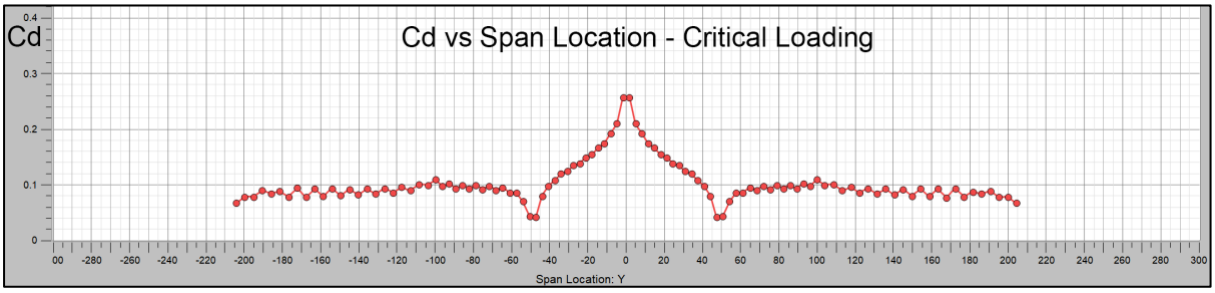

Figure 9: Drag Coefficient C_d vs Span Location – VSPAERO Result for Critical Loading Scenario

Scenario 3 – Landed

No aerodynamic forces act on the plane when it is stationary on the ground.

Data Processing and Loading Determination

The next step in obtaining the loading on the wings is to use the VSPAERO data to obtain the lift and drag force distributions over the wing.

Methodology:

1. The lift and drag coefficient data was imported into MATLAB.
2. As the data is symmetrical about the midpoint (both wings are identical) the data was trimmed to only include one wing.
3. The data was further trimmed such that any data points below 22.25” span location was discarded. This is because 22.25” is where the fuselage ends and the wing begins, making any points before that invalid.
4. The wing planform was described in MATLAB as a polygon using the previously determined geometry.
5. The planform polygon was segmented (sliced) into trapezoids according to the spanwise datapoints from VSPAERO.

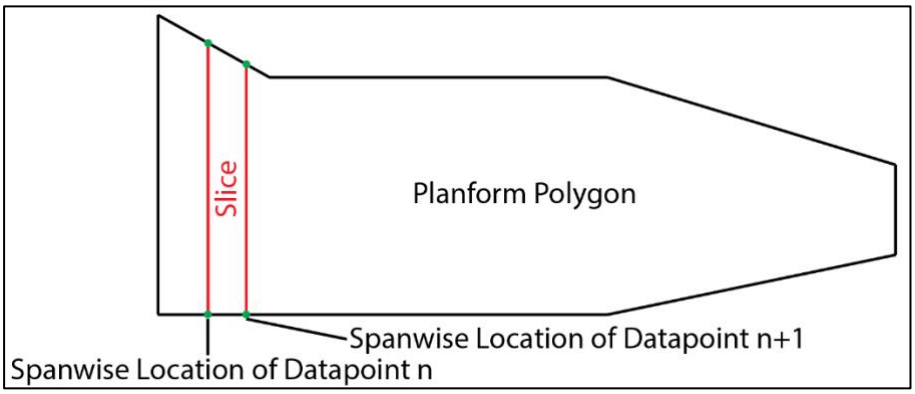

Figure 10: Illustration of Slicing the Planform Polygon According to the Spanwise Data

6. The area of each trapezoidal slice was determined.
7. The lift and drag force for each slice was then calculated using:

$$L_{slice} = C_{l,slice} \times q_\infty \times S_{slice}$$

$$D_{slice} = C_{d,slice} \times q_\infty \times S_{slice}$$

Authors: z5476963, z5479486, 5479091, z5481625, z5479578, z5676697

Where:

L_{slice} is the lift generated by the slice

$C_{l,slice}$ is the lift coefficient of the slice

D_{slice} is the drag generated by the slice

$C_{d,slice}$ is the drag coefficient of the slice

S_{slice} is the area of the slice

q_∞ is the dynamic pressure where $q_\infty = \frac{1}{2}\rho_{air}v^2$ (v is the velocity)

8. The slice lift and drag force were then divided by the spanwise distance between the datapoints used to create the slice to give the distributed lift and drag for that slice.
9. A polynomial regression was used to produce a function for the distributed lift and drag over the entire wing using all the slices. The polynomial degree was adjusted to yield a fit with a high R^2 value.
10. Further boundary conditions such as the weight of the fuel and the self-weight of the wing were taken into consideration as outlined below:

It is known that each wing has a 24-gallon fuel tank located between the spanwise points 57” and 88.75” (Piper Aircraft Corporation, 1994). It is assumed that the fuel acts as a point load, acting in the middle of the two points (70.25”) downwards. The most common fuel used for the Piper Archer II is 100LL (low lead), which has a density of 6.02 pounds per gallon. This means that each fuel tank weighs 144 lb.
It is known that each wing has a 24-gallon fuel tank located between the spanwise points $57''$ and $88.75''$ (Al-Shamma & Ali, 2014). It is assumed that the fuel acts as a point load, acting in the middle of the two points ($70.25''$) downwards. The most common fuel for the Piper Archer II is 100LL (low lead), which has a density of 6.02 pounds per gallon. This means that each fuel tank weighs $144\ lb$.

The empty wight of the Piper Archer II is $1416\ lb$, meaning each wing weighs $120\ lb$ if the wings amount to 17% of the aircraft’s empty weight. Dividing this figure by the span of each wing (189.32”) gives an approximation for the distributed wight of the wing. The distributed self-weight of the wing was subtracted from the distributed lift to give the net distributed force. Using his methodology, free body diagrams (FBD) were produced for the different scenarios. These diagrams use the direction convention outlined in Figure 2: Analysis Direction Convention Used in this Report

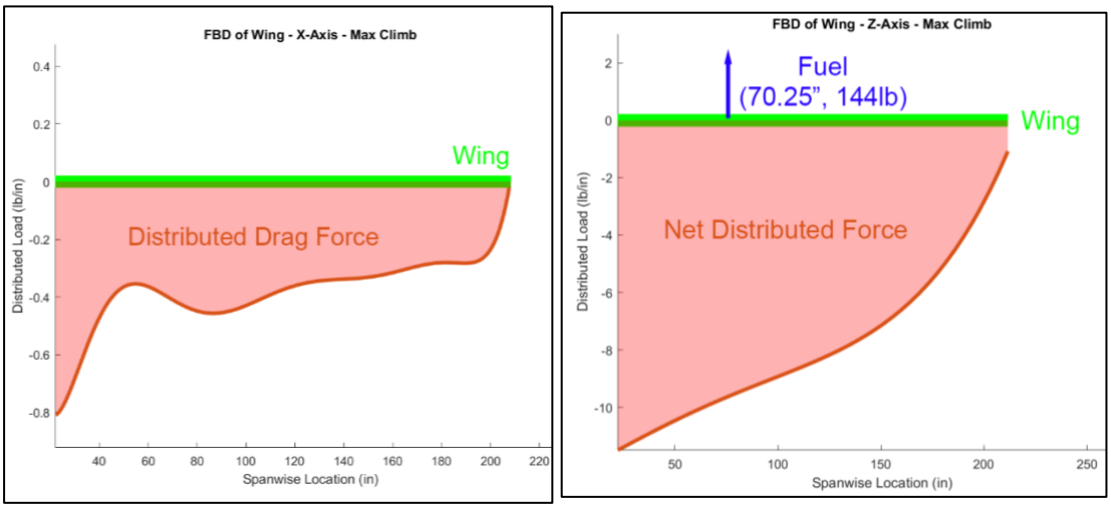

Figure 11 and Figure 12: Wing FBD’s in Z and X Respectively During Max Climb

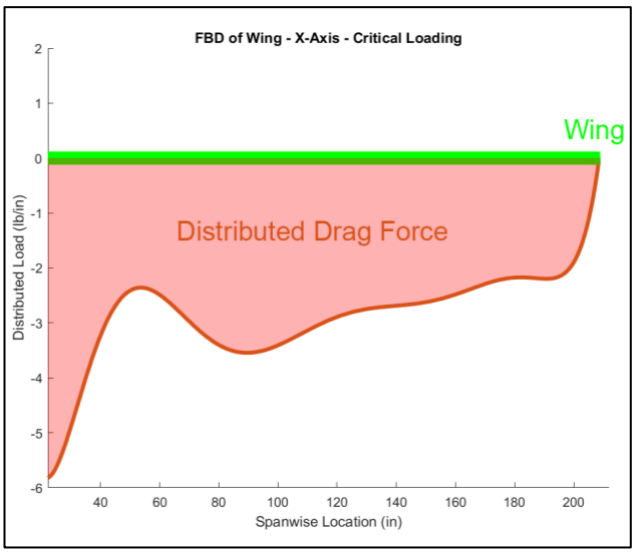

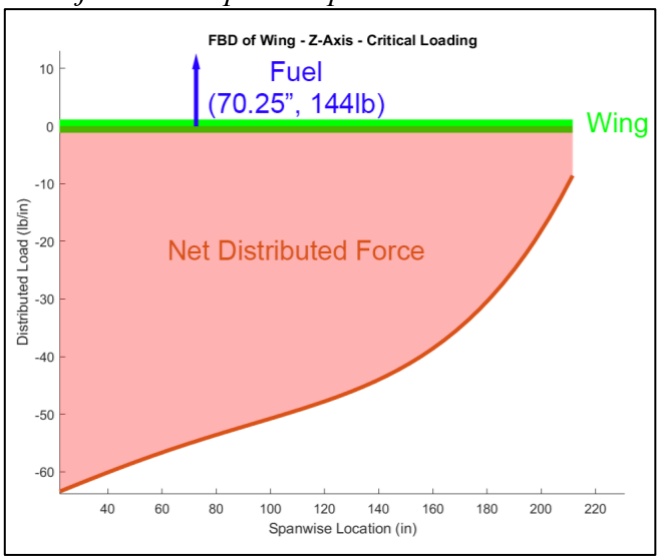

Figure 13 and Figure 14: Wing FBD's in Z and X Respectively During Critical Loading

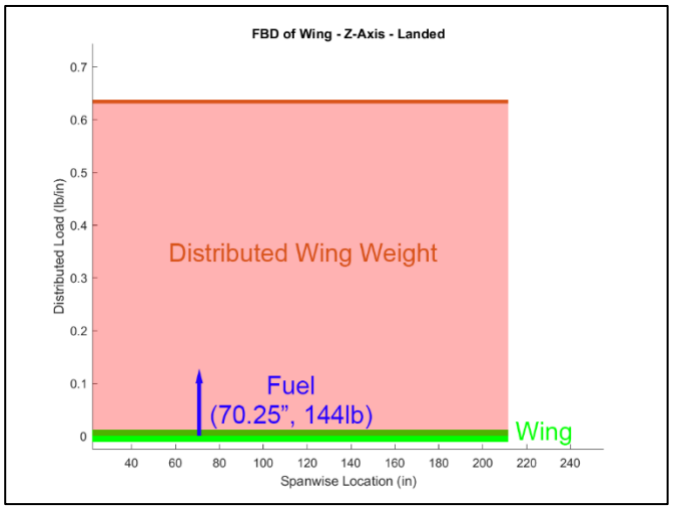

Figure 15: Wing FBD in Z While Landed

There are no loads in x while the plane is landed due to the lack of aerodynamic forces.

To determine the shear force and bending moment:

1. The distributed load was integrated along the span of the wing to obtain the corresponding shear force distribution.
2. If there were any point loads (such as the fuel), they were added to all the points before the load.
3. The resulting shear force distribution was then integrated again to produce the bending moment distribution.

Scenario 1 – Max Climb

Vertical shear force at root: $F_{z,max} = 1341\ lb$

Horizontal shear force at root: $F_{x,max} = 70.00\ lb$

Vertical bending moment at root $M_{z,max} = -1.075 \times 10^5\ lb \cdot in$

Horizontal bending moment at root $M_{x,max} = -5480\ lb \cdot in$

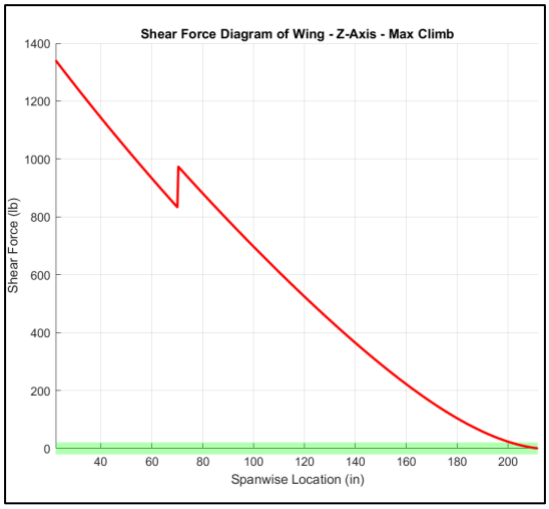

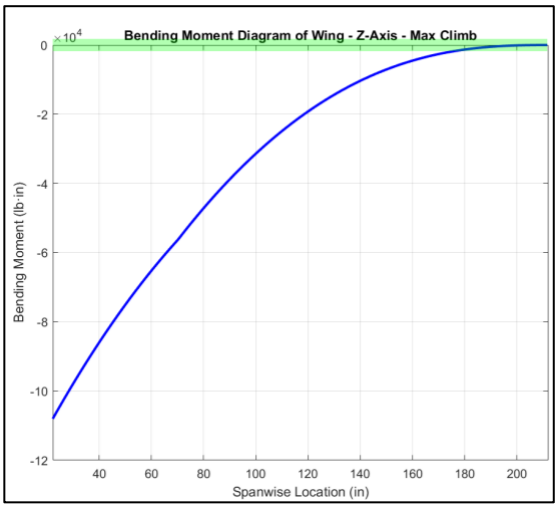

Figure 16 and Figure 17: Wing Vertical Shear Force and Bending Moment Diagrams During Max Climb. Wing in Green

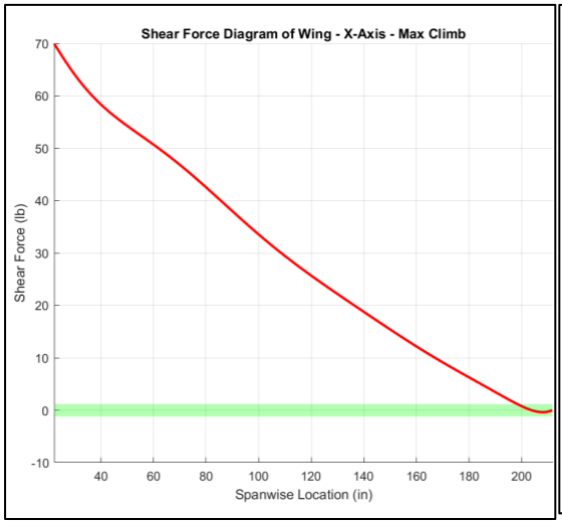

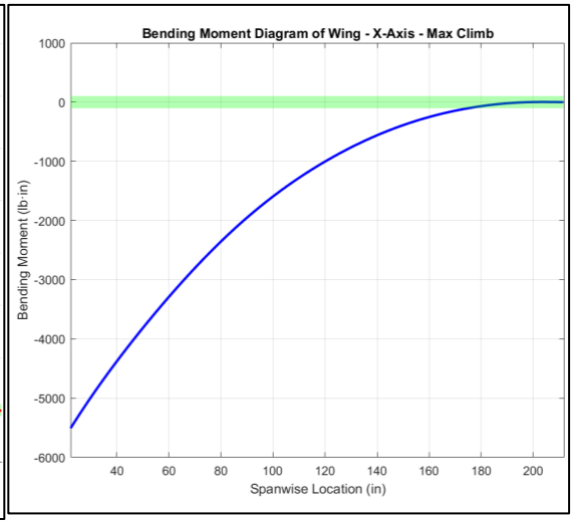

Figure 18 and Figure 19: Wing Horizontal Shear Force and Bending Moment Diagrams During Max Climb. Wing in Green

Authors: z5476963, z5479486, 5479091, z5481625, z5479578, z5676697

Scenario 2 – Critical Loading

Vertical shear force at root: $F_{z,max} = 8299\ lb$

Horizontal shear force at root: $F_{x,max} = 528.2\ lb$

Vertical bending moment at root $M_{z,max} = -6.567 \times 10^5\ lb \cdot in$

Horizontal bending moment at root $M_{x,max} = -43190\ lb \cdot in$

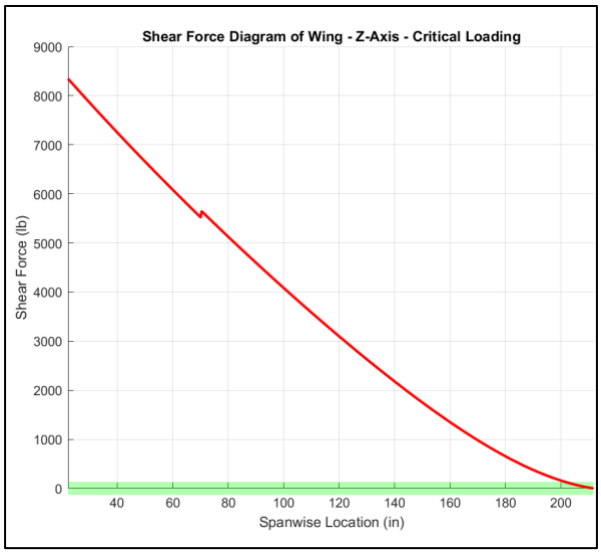

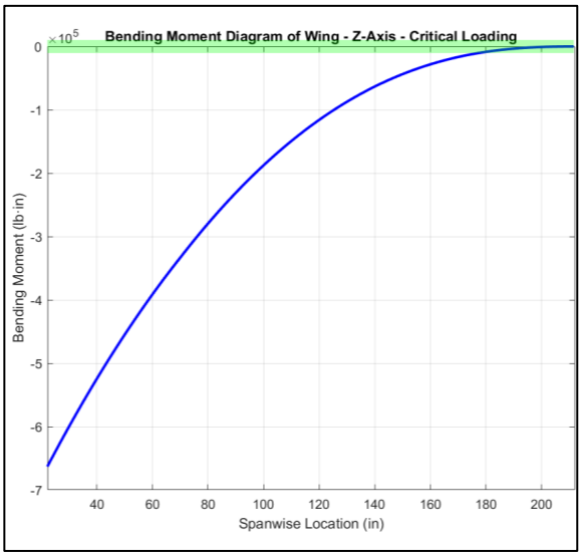

Figure 20 and Figure 21 – Wing Vertical Shear Force and Bending Moment Diagrams During Critical Loading. Wing in Green

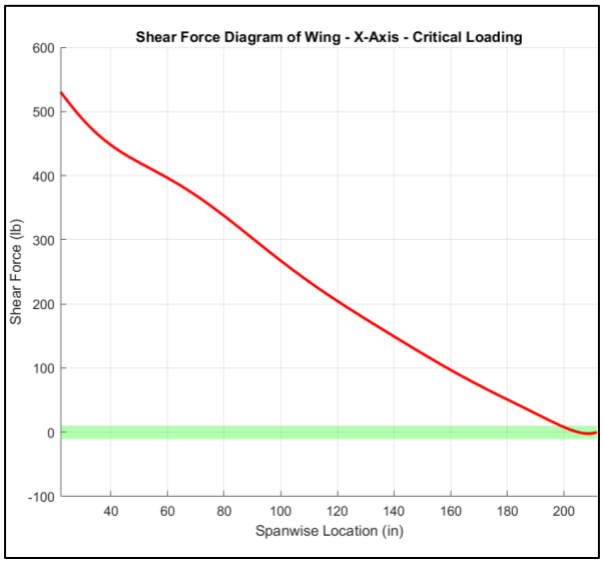

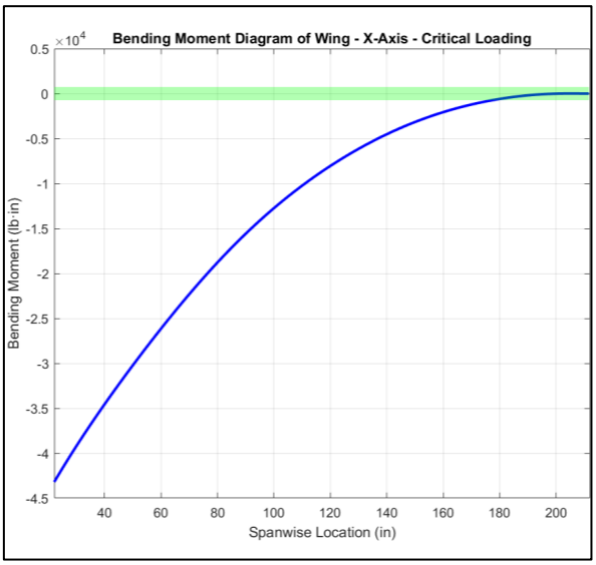

Figure 22 and Figure 23 – Wing Horizontal Shear Force and Bending Moment Diagrams During Critical Loading. Wing in Green

Authors: z5476963, z5479486, 5479091, z5481625, z5479578, z5676697

Scenario 3 – Landed

Vertical shear force at root: $F_{z,max} = -264\ lb$

Vertical bending moment at root $M_{z,max} = 1.817 \times 10^4\ lb \cdot in$

No forces or moments in x.

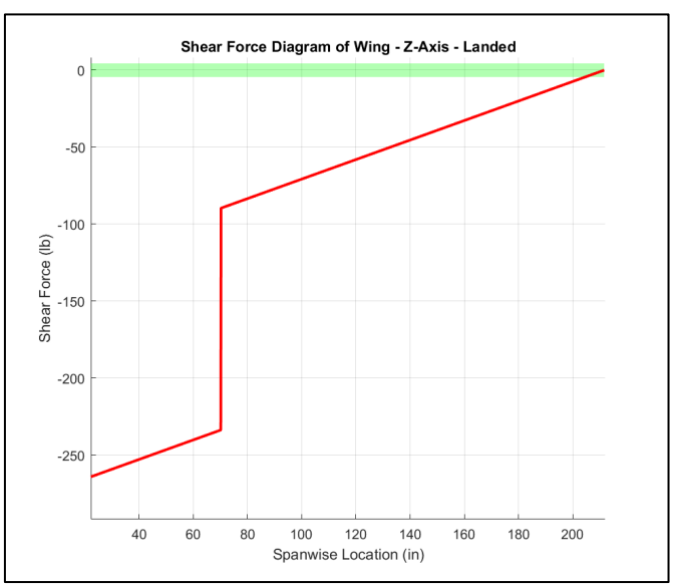

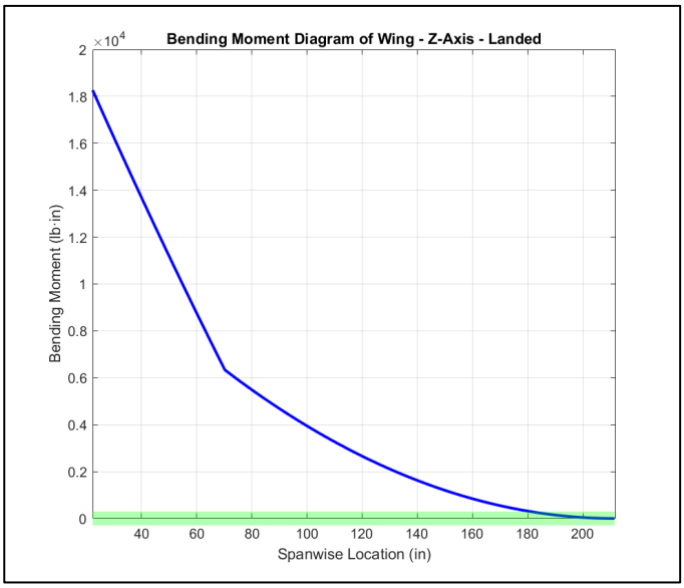

Figure 24 and Figure 25 – Wing Vertical Shear Force and Bending Moment Diagrams While Landed Wing in Green

The MATLAB code utilised can be found in Section 10 ‘

Directory of Supplementary Information'.

4.2 Fuselage Aerodynamic Loads and Centre of Pressure Determination

To determine the lift and drag on the fuselage in the respective load cases, COMSOL simulations were utilized to visualize and calculate the aerodynamic forces at the given plane velocity and angle of attack. A side view diagram of the Piper Archer II was traced in SolidWorks to output a DXF file of the outer structure of the fuselage. The COMSOL model simulates laminar fluid flow (in this case, the fluid is air) around the x-z cross section of the fuselage, similar to airfoil analysis. The model generates an air velocity field from the inlet boundary that simulates the direction of relative wind on the fuselage. The upper and lower boundaries of the model are open, and the right boundary is the outlet.

Lift and drag force are both determined by taking the integral of the pressure along the surface of the fuselage in the respective y and x directions using the expressions spf.T_stressy and spf.T_stressx. The COMSOL model solves for lift/drag force in N/m, which must be multiplied by the estimated width of the fuselage in the y-direction (41.25 in or 1.0478 m) to determine the area the lift and drag forces act over. An assumption is made that the fuselage cross-section along the y-axis is consistent, which is not entirely accurate as the fuselage is rounded along its sides; its y-cross section decreases in scale moving outward from the x-z plane. The lift and drag forces may be a slight over assumption from reality, though this model still provides an accurate assumption as the cabin geometry of the fuselage is relatively rectangular. For clarification, the lift and drag predicted in this model is generated by the fuselage only and does not include the lift and drag generated by the wings.

Centre of pressure was found by using the expression intop1(x*p)/intop1(p), which multiplies the surface pressure by its respective x-coordinate and divides it by total pressure along the surface of the fuselage. Lift and drag act from this centre of pressure in the free body diagrams.

Scenario 1: Max Climb

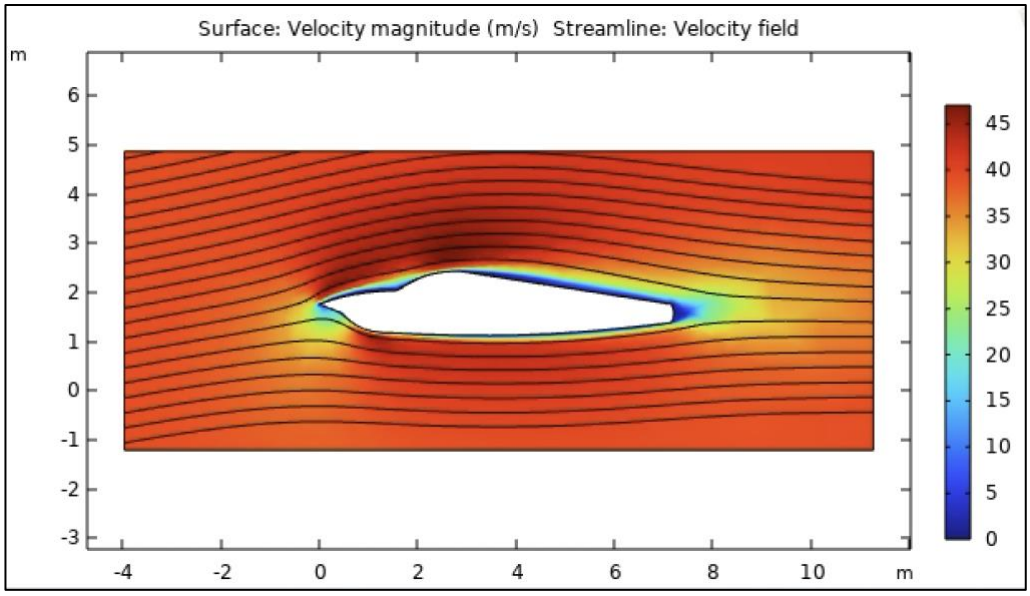

Figure 26: Velocity Field Surrounding Fuselage in Max Climb

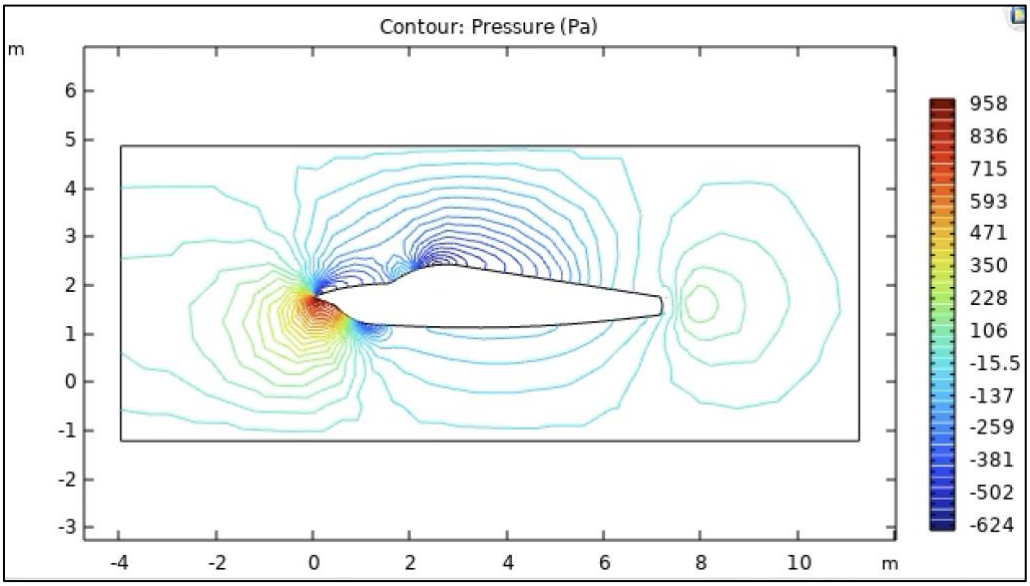

Figure 27: Contour Plot of Pressure on Fuselage Surface in Max Climb

Lift Force: $L = 2011.13\left(\frac{N}{m}\right) \times 1.0478 = 2107.26N = 437.73lb$

Drag Force: $D = 242.51\left(\frac{N}{m}\right) \times 1.0478 = 254.10N = 57.12lb$

Centre of Pressure: $142.9\ In$ from front tip

Scenario 2: Critical Loading

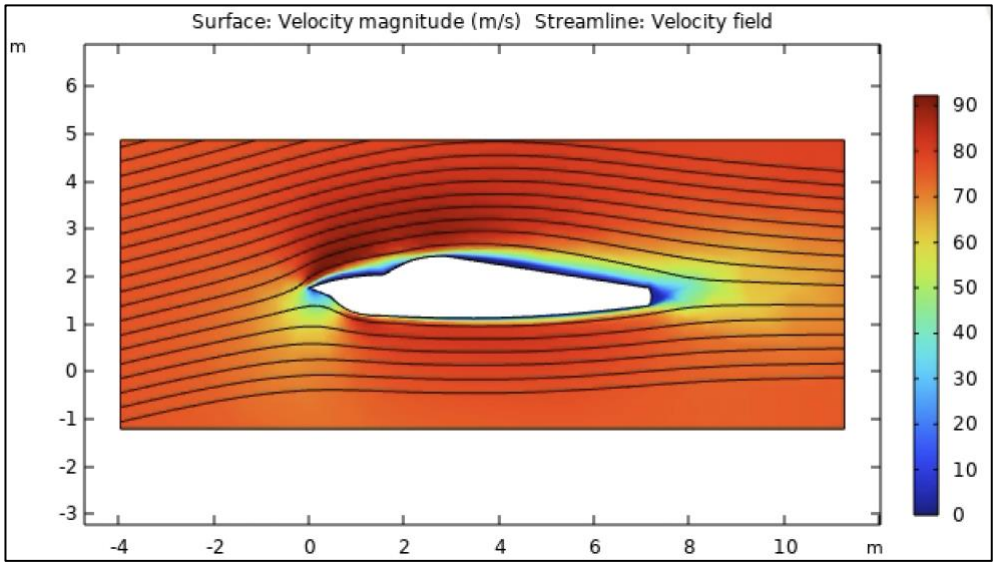

Figure 28: Velocity Field Surrounding Fuselage in Critical Loading

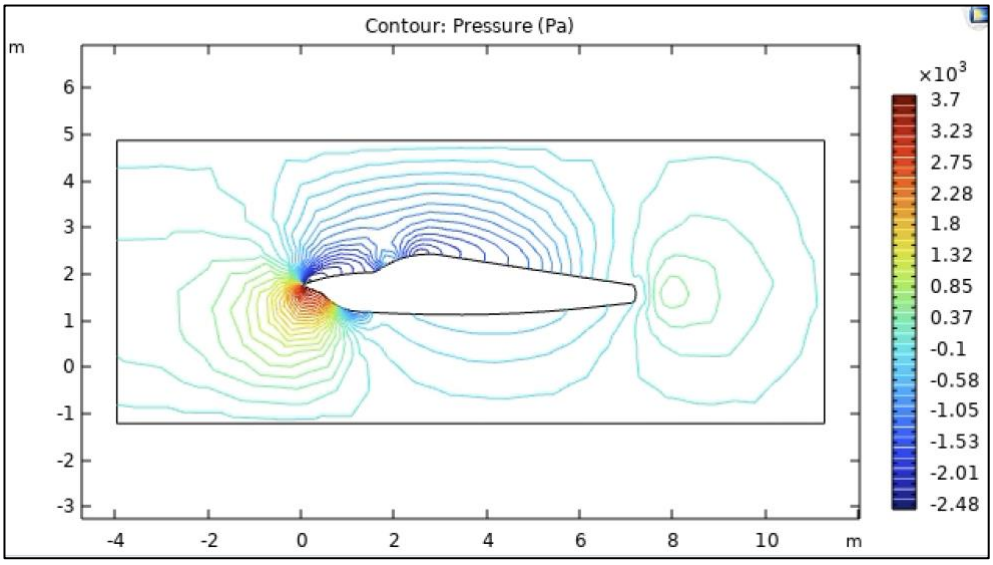

Figure 29: Contour Plot of Pressure on Fuselage Surface in Critical Loading

Lift Force: $L = 8828.9\left(\frac{N}{m}\right) \times 1.0478 = 9250.92N = 2079.69lb$

Drag Force: $D = 804.23\left(\frac{N}{m}\right) \times 1.0478 = 842.67ND = 804.23\left(\frac{N}{m}\right) \times 1.0478 = 842.67N = 189.44lb$

Centre of Pressure: 138.09 in from front tip

Scenario 3: Landed

Lift Force: N/A
Drag Force: N/A
Centre of Pressure: N/A

4.3 Fuselage Centre of Gravity Determination

The fuselage centre of gravity is necessary to determine the x-coordinate of the fuselage weight force. Fuselage weight could be derived by subtracting the wing weight from the total BEW of the aircraft.

Table 3: Fuselage Load Distribution

	Weight $(\boldsymbol{lbs})$	**Arm** $(\boldsymbol{inches})$	**Moment** $(\boldsymbol{lb-In})$
BEW	1176	88.4	103,958
Front Seat	310	80.5	24,955
Back seat passengers	310	118.1	36,611
Total	1796	-	165,524

$$CG = \frac{total\ M}{total\ W} = 92.26\ in$$

The values in Table 3 is gathered from Section 6.3 of (PILOT'S OPERATING HANDBOOK, 1975).

4.4 Free Body Diagrams

The vertical and horizontal shear forces at the wing root were calculated in the wing loading analysis in section 4.1- Wing Loading (page 8). Thrust, angle of attack (alpha), and pitch angle (theta) were predetermined in the load scenarios outlined in section 3.3– Load Cases (page 6). Aerodynamic loads act through the centre of pressure of the fuselage, which were both solved for in COMSOL (page 16). The weight force of the fuselage acts through the centre of gravity, and the shear forces from the wing base act at the wing centre (WC). The wing centre was derived from the distance from the nose to the centre of the main wheels (Piper Aircraft Corporation, 1994).

The Y-Z cross section of the fuselage is at the x-location of the wing centre, 109.7 in from the datum. The X-Z cross section of the fuselage cuts through the exact middle of the fuselage, where y=0.

Shear force and bending moment diagrams were generated by assuming the fuselage as a beam with a fixed boundary condition at the nose. The x-axis is always set to be the fuselage centreline, even with varying angles of attack.

Scenario 1: Max Climb

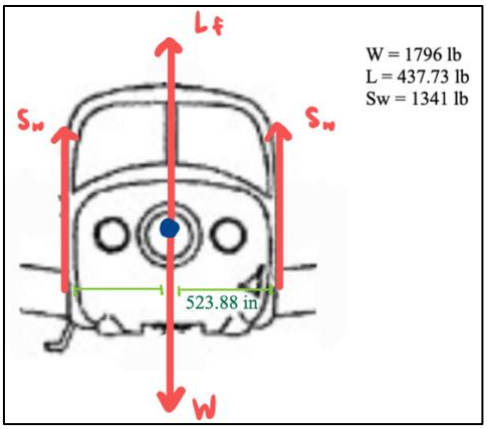

Figure 30: FBD of Y-Z Cross Section of Fuselage in Max Climb

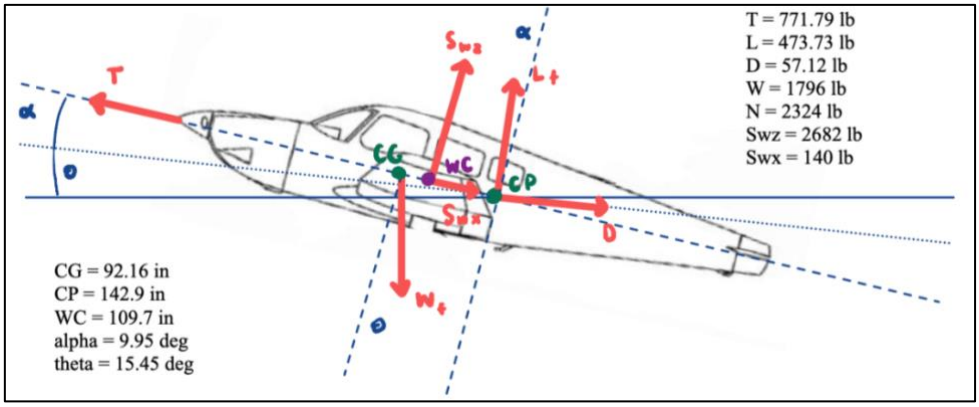

Figure 31: FBD of X-Z Cross Section of Fuselage in Max Climb

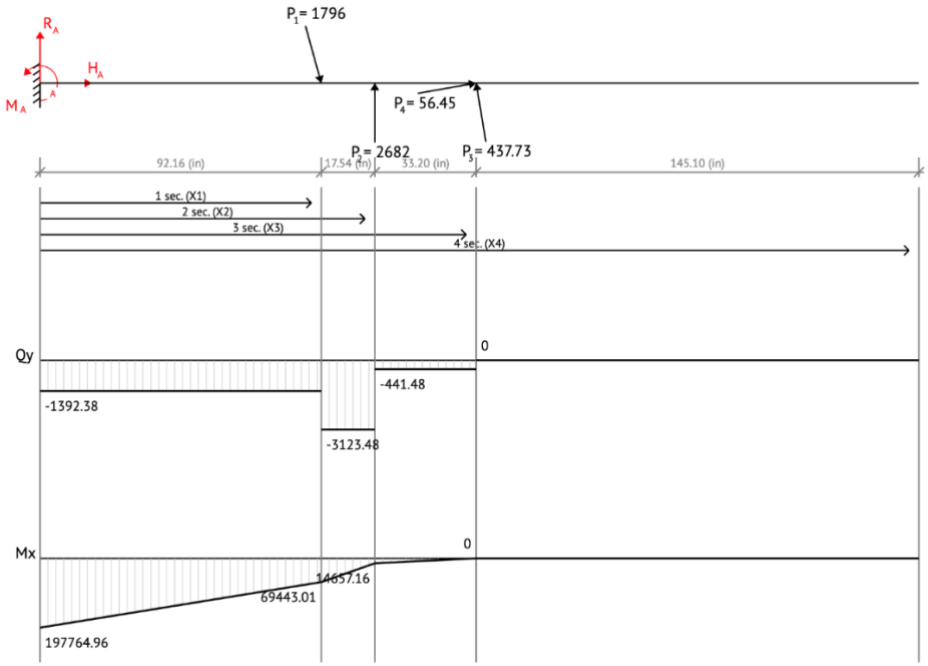

Figure 32:X-axis Shear Force and Bending Moment Diagram of Fuselage in Max Climb

Scenario 2: Critical Loading

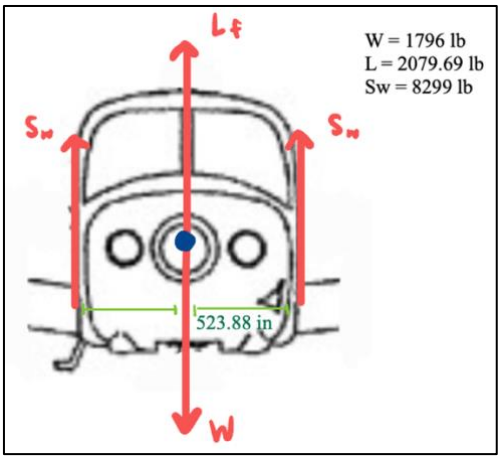

Figure 33: FBD of Y-Z Cross Section of Fuselage in Critical Loading

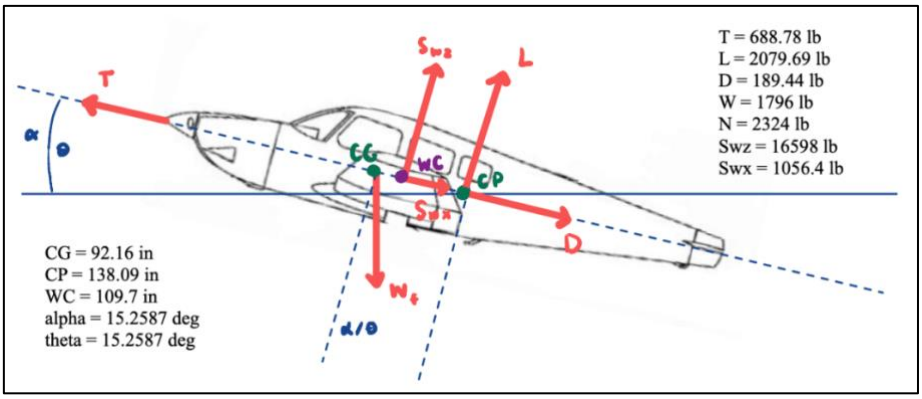

Figure 34: FBD of X-Z Cross Section of Fuselage in Critical Loading

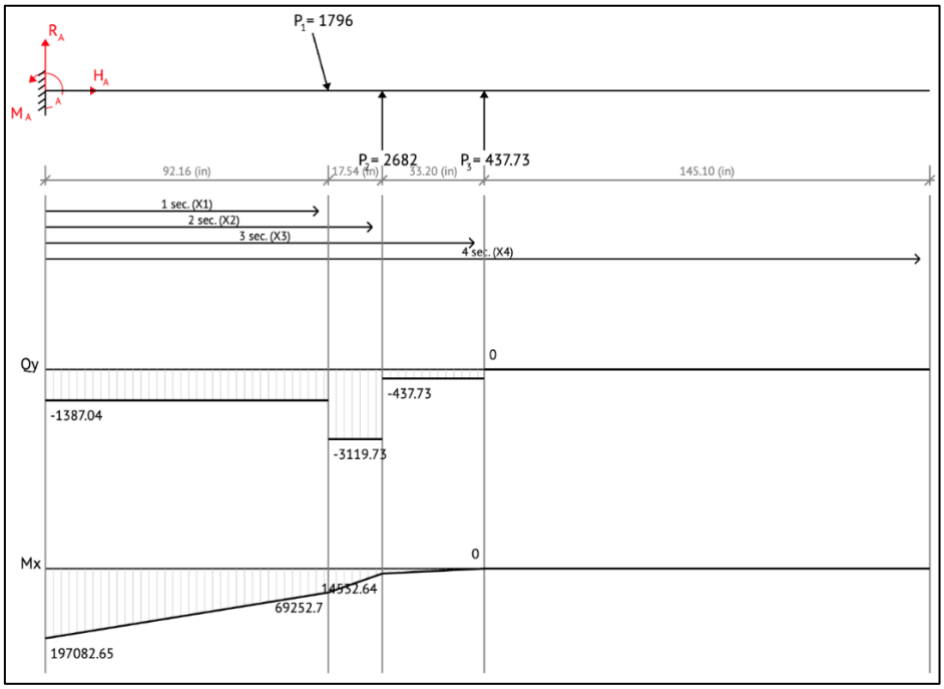

Figure 35: X-axis Shear Force and Bending Moment Diagram of Fuselage in Critical Loading

Authors: z5476963, z5479486, 5479091, z5481625, z5479578, z5676697

Scenario 3: Landed

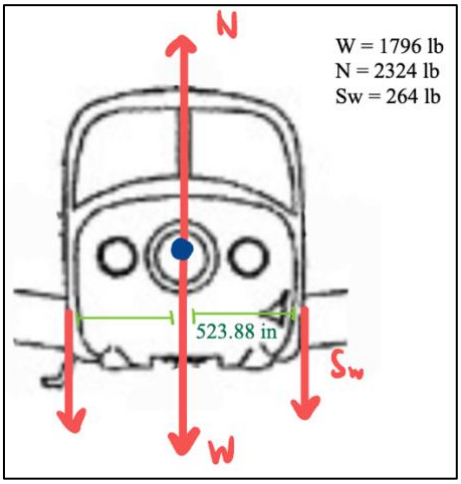

Figure 36: FBD of Y-Z Cross Section of Fuselage when Landed

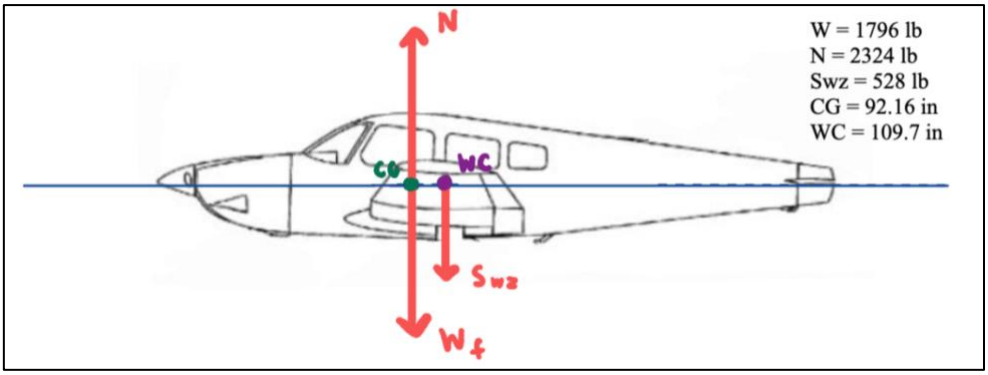

Figure 37:FBD of X-Z Cross Section of Fuselage when Landed

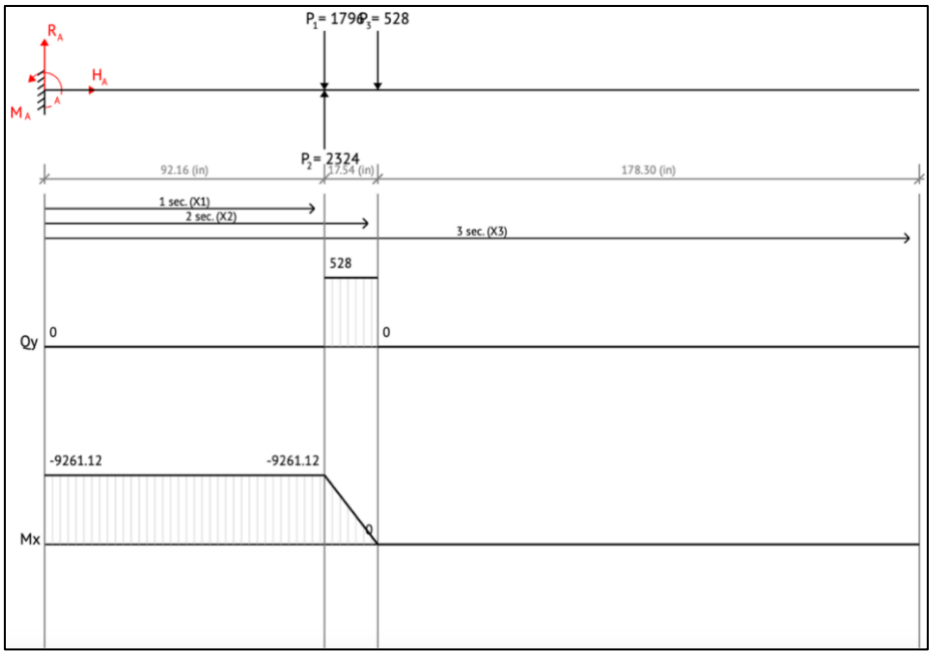

Figure 38 - X-axis Shear Force and Bending Moment Diagram of Fuselage when Landed

5 Empennage

5.1 Assumptions/Considerations

When analysing the load cases, we recognise that none of the specified cases involve turns. So, as we analyse the loads on the empennage, the vertical stabiliser can be ignored as aerodynamic forces will be negligible. Further, the main wing must be considered when determining the loads applied to the horizontal stabiliser as the downwash angle from the wing affects the effective angle of attack for the horizontal stabiliser. The elevator and its deflection angle is included when evaluating loads on the stabiliser.

5.2 Wing Geometry

In determining the geometry of the horizontal stabiliser, we take a similar approach to what was used for the wing previously whereby a scale drawing is placed as an image into SolidWorks so measurements can be taken from it.

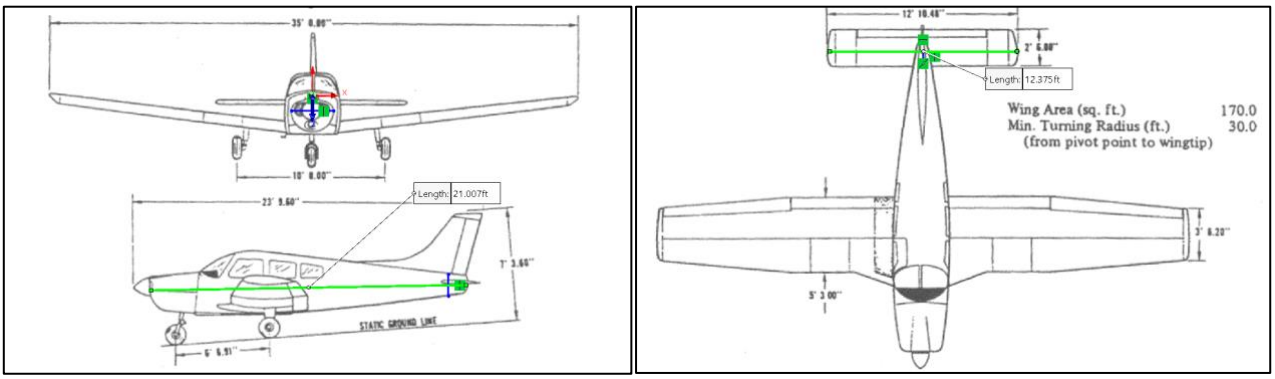

Figure 39: Scale Engineering Drawing Measurements

5.3 OpenVSP Analysis

As was done with the wing, the stabiliser was modelled parametrically in OpenVSP to be analysed.

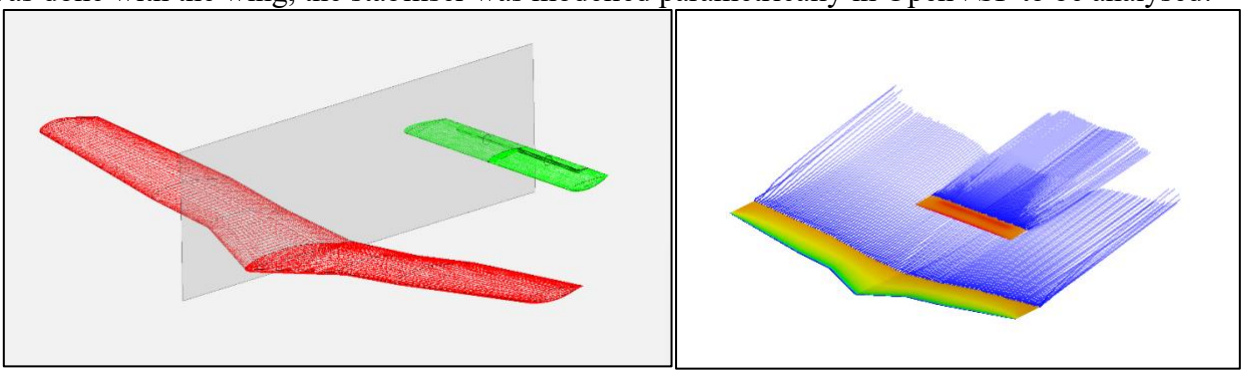

Figure 40: OpenVSP Geometry and Pressure and Trailing Wake Visualisation.

Analysing our aerofoils in VSPAERO, we can find accurate coefficients of lift and drag distributions across the length of the horizontal stabiliser. OpenVSP and VSPAERO also allow the addition of control surfaces that can easily be angled for different load cases. For our simulation, the elevator angle for max climb is estimated to be 12° and for critical loading 25°.

Scenario 1 – Maximum Climb

- Velocity: 39.1 m/s
- Angle of Attack: 9.95°
- Sea Level ($\rho_{air} = 1.225$ kg/m^3, $P = 101.35$ kPa, $c = 340.3$ m/s)
- Elevator Deflection Angle: 12°

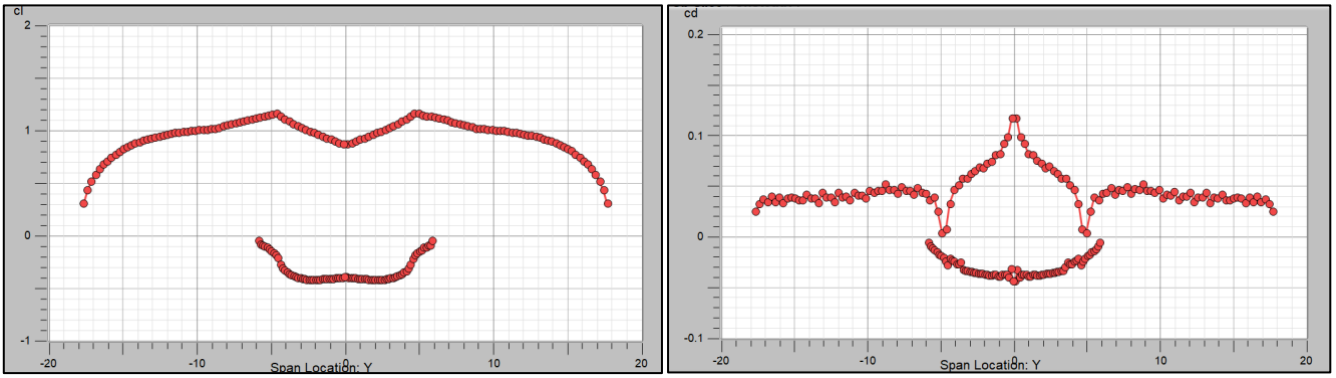

Figure 41: Maximum Climb CL and CD Diagrams.

Scenario 2 – Critical Loading

- Velocity: 76.4 m/s
- Angle of Attack: 15.26°
- Sea Level ($\rho_{air} = 1.225$ kg/m^3, $P = 101.35$ kPa, $c = 340.3$ m/s)
- Elevator Deflection Angle: 25°

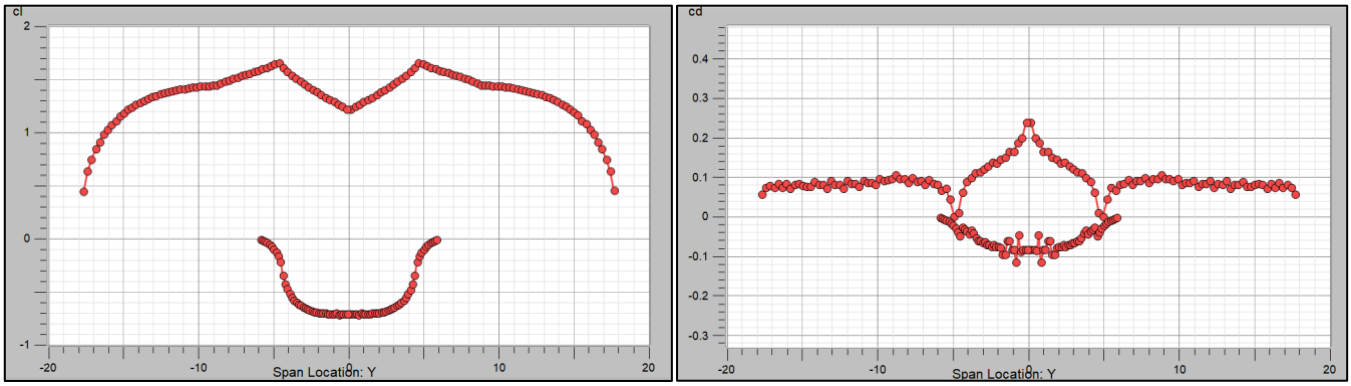

Figure 42: Critical Loading CL and CD Diagrams.

5.4 Data Processing and Loading Determination

The same methodology as the wing was used to process the data from VSPAERO and determine the loadings for the horizontal stabilizer. For this case, the data needed to be trimmed more to remove the main wing. The main wing was included in the VSPAERO simulation as the program accounts for the change in effective angle of attack seen by the horizontal stabiliser due to the downwash from the main wing, as well as any vortices it causes.

Scenario 1 – Max Climb

Vertical shear force at root: $F_{z,max} = 10.81\ N$

Horizontal shear force at root: $F_{x,max} = 0.66\ N$

Vertical bending moment at root: $M_{z,max} = -9.98\ Nm$

Horizontal bending moment at root: $M_{z,max} = -0.68\ Nm$

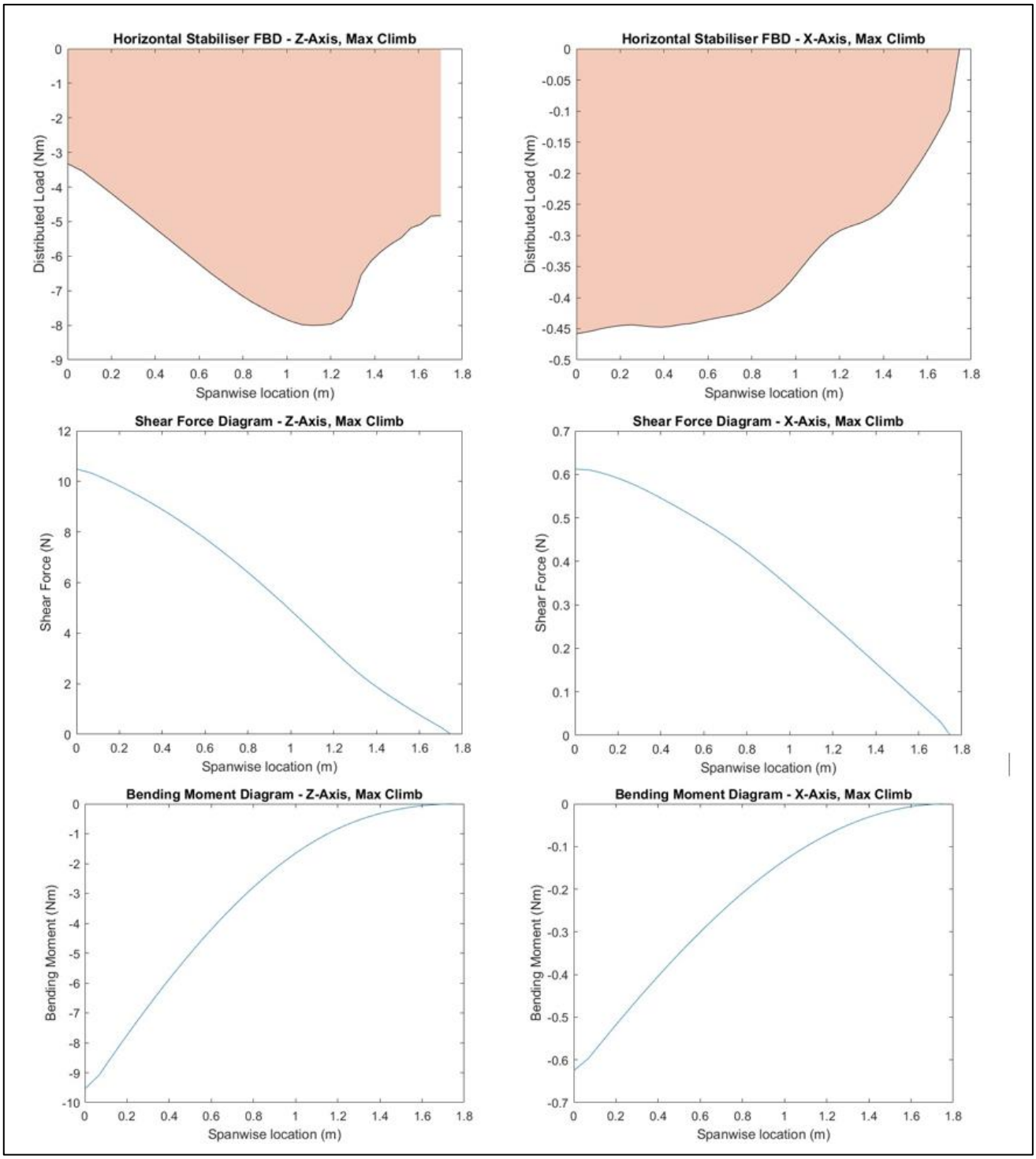

Figure 43: Maximum Climb FBD, SFD and BMD along Z and X Axes.

Scenario 2 – Critical Loading
Vertical shear force at root: $F_{z,max} = 13.05\ N$
Horizontal shear force at root: $F_{x,max} = 1.18\ N$
Vertical bending moment at root: $M_{z,max} = -11.43\ Nm$
Horizontal bending moment at root: $M_{z,max} = -1.29\ Nm$

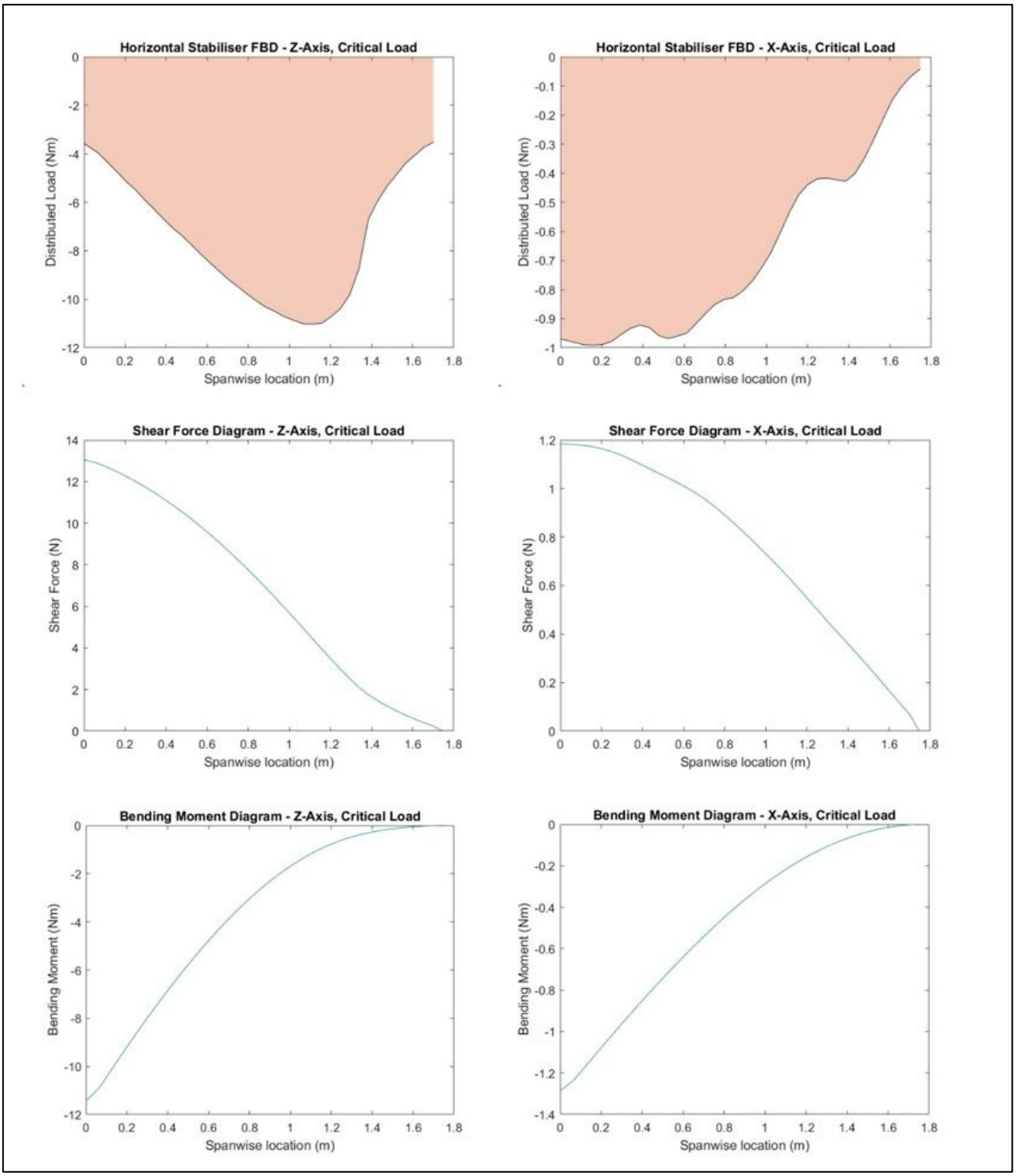

Figure 44: Critical Load FBD, SFD and BMD along Z and X Axes.

6 Stress Analysis

6.1 Wing

To analyse the wing section, the geometry needs to be idealised direct stress carrying booms and shear stress carrying panels. From Section 7.3 of the, (Piper Aircraft Corporations, 1975) we know that "the main spar is located under the rear seats". From Table 3, the rear seats are 118.1 inches from the datum, and from Section 6.3 of the same manual (Piper Aircraft Corporations, 1975), the leading edge of the wing is 78.4 inches away from the datum. Hence, the main spar is located 39.7 inched from the wing leading edge.

From Figure 1.1 of the manual, the max chord length is 63 inches; it is assumed that this chord length is constant as the shape of the wing is close to a rectangle. Hence, the main spar is located around 63% of chord.

The geometry of the wing section was estimated by comparing it to similar studies. The NASA composite wing box test structure (NASA STI Program Office, 2001) is used in many aerospace structural analysis studies for General aircrafts like the Piper Archer II. From these studies, the rib web was taken and idealised into this sketch.

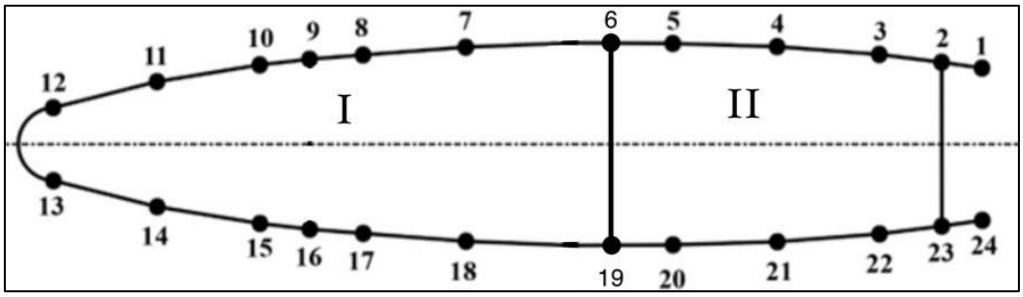

Figure 45 Idealised Boom-Panel Model of the Wing Section

To estimate the stresses at various points, the boom areas need to be calculated for each of the booms using the formula:

$$B = A_{stiffener} + \frac{t * l}{6}(2 + \frac{y_2}{y_1})$$

Where t is the skin thickness, from **Error! Reference source not found.** the $t = 0.025\ in.$ l is the length between the booms, and $\frac{y_2}{y_1}$ is the ratio of the distance of the two booms to the $\bar{y}$. For simplification, the length between the booms is assumed to be a straight line. Since the coordinates of each boom is known, the length is calculated using Pythagoras Theorem.

The area of the stiffener was estimated by comparing this aircraft to similar ones. Once again, the NASA composite wing box test structure (NASA STI Program Office, 2001) is used. From this study, the stiffener area was between $0.2\ in^2$ and $0.3\ in^2$. Comparing from these studies, the area of our stiffener was chosen to be $A_{stiffener} = 0.248\ in^2$.

Using the equation, the Boom area for each of the booms are evaluated and shown in Table 4.

Table 4: Data for the Boom Points

Boom	x (in)	y (in)	Area (in^2)
1	0	1.50669303	0.2766265862
2	2.283959947	1.518897756	0.3044606316
3	6.612507085	1.717126118	0.3328925986
4	13.22501417	1.856496207	0.3316730001
5	19.83752125	1.92500015	0.2912677066
6	23.3	1.923228496	0.3685036945
7	33.06253542	1.850984396	0.3285290564
8	39.67504251	1.708070999	0.2835776861
9	42.59380314	1.580708784	0.2934415913
10	46.28754959	1.505708778	0.324972297
11	52.90005668	1.195078833	0.3327240078
12	61.23313811	0.5259842928	0.248
13	61.23313811	-0.5259842928	0.09966834377
14	52.90005668	-1.195078833	0.1581821997
15	46.28754959	-1.505708778	0.2010615563
16	42.59380314	-1.580708784	0.2105356052
17	39.67504251	-1.708070999	0.1630383907
18	33.06253542	-1.850984396	0.1243806709
19	23.3	-1.923228496	0.2047057257
20	19.83752125	-1.92500015	0.1663241436
21	13.22501417	-1.856496207	0.1674120419
22	6.612507085	-1.717126118	0.1959752269
23	2.283959947	-1.518897756	0.2195269681
24	0	-1.50669303	0.248

The x values are the distance the boom points are away from the datum, which is the far right of the idealised sketch. The y values are the distance the boom points are away from the centre line.

The second moment of area could now be calculated for the idealised sketch. Since there is a horizontal symmetry, $I_{xy} = 0$. The equation for the second moment of area about x is:

$$I_{xx} = \sum By^2$$

From
Table 4, these values are obtained, and the second moment of area is:

$$I_{xx} = 33.02\ in^4$$

And the second moment of area about y is:

$$I_{yy} = \sum Bx^2$$

Where x is the horizontal distance between the centroid and the boom point.

$\bar{x}$ can be found using the equation:

$$\bar{x} = \frac{\sum Bx}{\sum B} = 28.02\ in$$

This value is from the datum. Now the second moment of around y is calculated:

$$I_{yy} = 4157.04\ in^4$$

The idealised sketch is assumed to be a rectangle and a trapezoid to calculate the area of each of the cells. From this estimation, the area of the cells is:

$$A_I = 110.52\ in^2$$
$$A_{II} = 78.03\ in^2$$

Now the shear flow analysis can be made using the following equation for each of the flows. An example of this equation for the first panel is:

$$BE1 = q_{12} - q_0 = -\frac{S_y}{I_{xx}} B_1 y_1 - \frac{S_x}{I_{yy}} B_2 x_2$$

The boom equations are written for each of the flows and now the Rate of twist equations needs to be written for the two cells:

$$ROT = \frac{d\theta}{dz} = \frac{1}{2[A]G} \sum q\delta$$

The rate of twist, $\frac{d\theta}{dz}$ is assumed to be zero. [A] is the enclosed area of the cell, which was calculated previously. G is the shear modulus; in this case it is $G = 4060\ ksi$, q is the shear flow and δ is found using:

$$\delta = \frac{s}{t}$$

Where s is the length of the panel of each boom. δ coefficients are different for each panel. To find the length, it is assumed that the line between each boom point is a straight line. Then the Pythagoras theorem is used. The panel 12-13 will not be assumed to be a straight line, it will be assumed to be a semi-circle. The δ coefficients for each of the panels are calculated and shown in

Table 5:

Table 5: Delta Coefficients for each Panel

	x (in)	y (in)	s (in)	δ coefficients -
01-02	0	1.50669303	2.283992556	91.35970223
02-03	2.283959947	1.518897756	4.333083753	173.3233501
03-04	6.612507085	1.717126118	6.612861917	264.5590262
04-05	13.22501417	1.856496207	6.612861917	264.5144767
05-06	19.83752125	1.92500015	3.462479199	138.4991679
06-07	23.3	1.923228496	9.762802729	390.5121091
07-08	33.06253542	1.850984396	6.614051269	264.5620508
08-09	39.67504251	1.708070999	2.921538077	116.8615231
09-10	42.59380314	1.580708784	3.694507801	147.7803121
10-11	46.28754959	1.505708778	6.619799159	264.7919664
11-12	52.90005668	1.195078833	8.359900334	334.3960134
12-13	61.23313811	0.5259842928	1.65242839	66.0971356
13-14	61.23313811	-0.5259842928	8.359900334	334.3960134
14-15	52.90005668	-1.195078833	6.619799159	264.7919664
15-16	46.28754959	-1.505708778	3.694507801	147.7803121
16-17	42.59380314	-1.580708784	2.921538077	116.8615231
17-18	39.67504251	-1.708070999	6.614051269	264.5620508
18-19	33.06253542	-1.850984396	9.762802729	390.5121091
19-20	23.3	-1.923228496	3.462479199	138.4991679
20-21	19.83752125	-1.92500015	6.612861917	264.5144767
21-22	13.22501417	-1.856496207	6.613975655	264.5590262
22-23	6.612507085	-1.717126118	4.333083753	173.3233501
23-24	2.283959947	-1.518897756	2.283992556	91.35970223
02-23	2.283959947	1.518897756	3.037795512	121.5118205
06-19	23.3	1.923228496	3.846456992	153.8582797

Using the δ coefficients, the rate of twist equations can be formed for the two cells.
Next, the torque equations can be formed. The torque equation is:

$$TE = S_y\xi - S_x\eta = 2\sum[A]q$$

Where S_y, is the vertical loading and S_x, is the horizontal loading. ξ is the horizontal distance of the shear center from the reference point, and η is the vertical distance of the shear center from the reference. Hence the shear center is the coordinate (ξ, η) from the reference. The vertical distance of the shear center is at the middle of the idealised system as it is assumed to be symmetrical.

The $[A]$ is the triangular area of the chosen reference point makes with the two boom points the shear is flowing from. The reference point of the torque is chosen to be boom 19. The distance between the boom points is also approximated to be a straight line to make the area calculations simplified. The formula for area of a triangular given the length of all the sides is:

$$A = \frac{1}{4}\sqrt{4a^2b^2 - (a^2 + b^2 - c^2)^2}$$

The location of the boom points is all known, hence the length of the sides is calculated using Pythagoras theorem. Using the area of the triangle formula, all the triangular areas are found. Hence the Torque equation is written in MATLAB.

From this, the torque equation is written in the MATLAB code. From this analysis, there are 23 boom equations, two rate of twist equations and one torque equation. The unknowns are the shear flow along each boom point, and the shear center. These unknows are calculated and the code named 'shear_flow_calculations'.

This calculation is used for all the load cases, max climb, critical loading, and landed.

The shear stress for each of the panels is then calculated using the formula:

$$\tau = \frac{q}{t}$$

Where q is the shear flow between each boom point, and t is the thickness. From the equations formed the shear flow and shear stress are:

Table 6: Shear Flow and Shear Stress for the three Scenarios

Panel	Shear flow Max Climb (lb/in)	Shear Stress Max Climb (psi)	Shear flow Critical (lb/in)	Shear Stress Critical (psi)	Shear Flow Landed (lb/in)	Shear Stress Landed (psi)
01-02	-17.057	-682.284	-105.738	-4229.52	3.33231	133.2924
02-03	72.812	2912.46	450.375	18015	-14.3677	-574.708
03-04	49.477	1979.08	305.803	12232.12	-9.79752	-391.9008
04-05	24.388	975.508	150.422	6016.88	-4.87451	-194.9804
05-06	1.577	63.08	9.19948	367.9792	-0.3917	-15.668
06-07	58.6958	2347.832	362.649	14505.96	-11.6423	-465.692
07-08	34.0276	1361.104	210.024	8400.96	-6.7804	-271.216
08-09	14.4121	576.484	88.7059	3548.236	-2.90778	-116.3112
09-10	-4.3534	-174.136	-27.3302	-1093.208	0.800742	32.02968
10-11	-24.1254	-965.016	-149.556	-5982.24	4.71288	188.5152
11-12	-40.1345	-1605.38	-248.442	-9937.68	7.892	315.68
12-13	-45.2933	-1811.73	-280.18	-11207.2	8.93493	357.3972
13-14	-43.1086	-1724.34	-266.584	-10663.36	8.51579	340.6316
14-15	-35.3651	-1414.60	-218.572	-8742.88	7.00438	280.1752
15-16	-23.0084	-920.336	-142.017	-5680.68	4.58393	183.3572
16-17	-9.4413	-377.652	-57.9847	-2319.388	1.92318	76.9272
17-18	1.9003	76.012	12.2481	489.924	-0.303324	-12.13296
18-19	11.2608	450.432	70.1913	2807.652	-2.14402	-85.7608
19-20	-58.6972	-2347.89	-362.777	-14511.08	11.6252	465.008
20-21	-45.7173	-1828.69	-282.48	-11299.2	9.06535	362.614
21-22	-33.1368	-1325.47	-204.681	-8187.24	6.58045	263.218
22-23	-19.5411	-781.644	-120.637	-4825.48	3.88997	155.5988
23-24	-114.8759	-4595.036	-710.887	-28435.48	22.6214	904.856
02-23	-108.7812	-4351.248	-673.336	-26933.44	21.3973	855.892
06-19	-85.9303	-3437.212	-531.795	-21271.8	16.9169	676.676

6.2 Bending Stress

Using the loading calculated for the three scenarios, the Moment at each boom point is calculated. There is loading in two directions, hence the total moment consists of the superposition of both the loadings. The Moment at each boom point is calculated by using:

$$M_{total} = S_x y + S_y x$$

Where y is the vertical distance of the boom point from the centroid, and x is the horizontal distance of the boom point from the centroid. From the total Moment, the total bending stress at the boom can be calculated using the equation:

$$\sigma = \frac{M_x y}{I_{xx}} + \frac{M_y x}{I_{yy}}$$

This equation is used for all the boom points for the three scenarios, and is evaluated to be:

Table 7: Bending stress for the 3 Scenarios

Boom	M_{total} Max Climb (lb-in)	σ Max Climb (psi)	M_{total} Critical Load (lb-in)	σ Critical Load (psi)	M_{total} Landed (lb-in)	σ Landed (psi)
1	3651.48	1426.31	24811.11	8827.73	-397.77	-280.68
2	3507.96	1296.91	23706.00	8026.90	-400.99	-255.22
3	3470.79	1164.19	23064.76	7205.46	-453.32	-229.10
4	3194.81	759.92	20728.67	4703.34	-490.11	-149.54
5	2823.80	270.80	17804.46	1676.05	-508.20	-53.29
6	2579.05	0	15960.87	0	-507.73	0
7	3165.55	734.17	20517.89	4543.95	-488.66	-144.47
8	3436.78	1136.37	22824.58	7033.26	-450.93	-223.62
9	3470.30	1239.09	23309.29	7668.99	-417.31	-243.84
10	3628.28	1406.26	24637.90	8703.66	-397.51	-276.73
11	3674.60	1437.21	25552.71	8895.23	-315.50	-282.82
12	3360.66	810.63	24401.43	5017.18	-138.86	-159.52
13	1949.97	-810.63	15671.14	-5017.18	138.86	159.52
14	469.40	-1437.21	5716.79	-8895.23	315.50	282.82
15	-410.03	-1406.26	-353.85	-8703.66	397.51	276.73
16	-769.16	-1239.09	-2927.32	-7668.99	417.31	243.84
17	-1144.27	-1136.37	-5525.98	-7033.26	450.93	223.62
18	-1798.79	-734.17	-10204.75	-4543.95	488.66	144.47
19	-2579.05	0	-15960.87	0	507.73	0
20	-2339.05	-270.80	-14146.69	-1676.05	508.20	53.29
21	-1784.31	-759.92	-10085.45	-4703.34	490.11	149.54
22	-1134.54	-1164.19	-5436.10	-7205.46	453.32	229.10
23	-565.72	-1296.91	-1504.66	-8026.89582	400.99	255.22
24	-389.47	-1426.31	-196.99	-8827.73	397.77	280.68

6.3 Fuselage

For bending stress and shear stress analysis, the cross-section of the fuselage in the Y-Z plane (located at the x-coordinate of the wing centre) needs to be idealized to a boom-and-panel structure. The cross-section is simplified to a circle with a diameter equal to the average cabin height and width of the fuselage (43.366 in) (Piper Aircraft Corporation). The structure contains 16 booms with stiffeners at booms 2, 3, 5, 7-11, 13, 15, and 16, in an attempt to best model the placement of actual stiffeners in the plane fuselage (Piper Aircraft Corporation, 1994). The skin thickness is 0.032 inches, found from Piper Archer II's parts catalogue (Piper Aircraft Corporation, 1994). No specific dimensions were found for the cross-sectional geometry of each stiffener, so each stiffener was estimated to be 0.6948 inches squared. This estimation was found using an engineering drawing of a fuselage stiffener (Figure 52 Possible stiffener option) that had a similar-shaped cross section to the stiffeners pictured in the parts catalogue below.

As seen in the lower forward cockpit assembly below (Piper Aircraft Corporation, 1994), a large spar box of index number 24 positioned across the cross-section of the fuselage presumably takes on a significant portion of the shear loading from the wing bases, and the spar box is not accounted for in this simplified model. Therefore, this fuselage loading analysis may significantly overestimate the amount of shear loading taken on by the fuselage skin and stiffeners themselves.

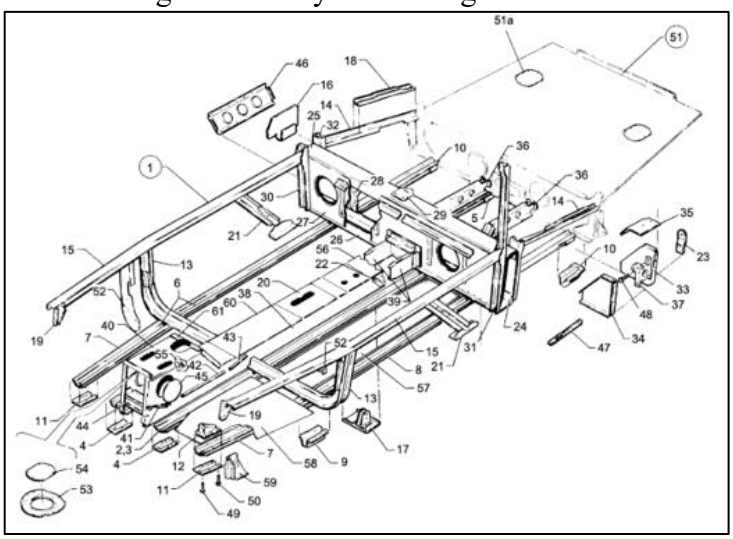

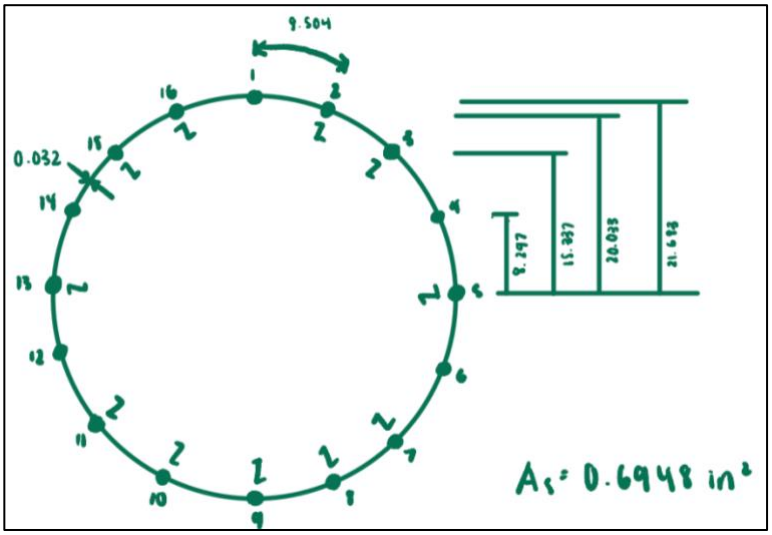

Figure 46 – Fuselage Lower Forward Cockpit Assembly, Idealised Fuselage Cross Section Drawing

Table 8: Locations and Areas of each Boom

Boom	x (in)	y (in)	Area (in^2)
1	0	21.683	175.79
2	8.297	20.033	624.05
3	15.337	15.337	624.05
4	20.033	8.297	175.79
5	21.683	0	624.05
6	20.033	-8.297	175.79
7	15.337	-15.337	624.05
8	8.297	-20.033	624.05
9	0	-21.683	624.05
10	-8.297	-20.033	624.05
11	-15.337	-15.337	624.05
12	-20.033	-8.297	175.79
13	-21.683	0	624.05
14	-20.033	8.297	175.79
15	-15.337	15.337	624.05
16	-8.297	20.033	624.05

Fuselage Shear Force and Bending Stress Analysis

Since thrust and drag work perpendicular to the fuselage cross-section, the only significant forces contributing to shear stress on the fuselage are the shear forces at the wing bases. The aircraft is not pressurized, so there is no internal pressure causing radial shear stress. Bending moment, necessary to calculate bending stress, can be found by identifying the point on the bending moment diagram for each respective load case, where the x-coordinate along the fuselage is equal to the wing centre. A MATLAB script was employed to calculate both of these stress values for each panel and boom.

Necessary for finding the shear or bending stress at each boom, the second moments of area about the x and y axis of the structure were evaluated by summing the individual second moments of area for each boom.

$$I_{xx} = \sum B_i \cdot y_i^2$$

$$I_{yy} = \sum B_i \cdot x_i^2$$

To calculate the shear stress in each panel, the shear loads at each wing base were each evaluated individually, and the resulting shear stresses were superimposed to get the final shear stress calculations. Shear flow is assumed to be in the clockwise direction, hence the negative value for half of the panels of the fuselage.

To find the basic shear flows in each panel, the following formula was used.

$$q_{bi} = -\frac{S_y}{I_{xx}} \cdot \big(B(i) \cdot y(i)\big)$$

Next, to find constant shear flow along the fuselage, the following formula was used, with [A] being the total enclosed area of the cross-section. The torque is equal to the shear force times the distance of the force to the shear centre (20.625 in), which is half of the cabin width. Torque was applied in the negative direction when evaluating the second wing's shear flows.

$$q_{s0} = \frac{T_S - 2\sum(-q_b) * A_i}{[A]}$$

Finally, to find the final shear flows, constant shear was subtracted from basic shear for each panel.

$$q_{s(i)} = q_{b(i)} - q_{s0}$$

The previous formula generated an array of shear flows, which could be converted into shear stresses by dividing by the panel thickness.

$$\tau_i = \frac{q_{s(i)}}{t}$$

Secondly, to find the bending stress in each boom, the bending moment was identified for each load case by finding the corresponding y-value to the x-value of the wing centre on the bending moment diagram (22.72 lb-in for max climb, 91.55 lb-in for critical load, 0 lb-in for landed). Bending stress was found by multiplying bending moment by the y-value of each boom and dividing by the second moment of area about the x-axis.

$$\sigma_{z(i)} = \frac{M_x \cdot y_i}{I_{xx}}$$

Table 9: Shear Stress for the three Scenarios

Boom	Shear Stress Max Climb (psi)	Shear Stress Critical (psi)	Shear Stress Landed (psi)
1-2	-275.9637	-1742.9	55.4447
2-3	-785.9016	-4963.6	157.8981
3-4	-1176.2845	-7429.2	236.3311
4-5	-1235.7786	-7805	248.2843
5-6	-1235.7786	-7805	248.2843
6-7	-1176.2845	-7429.2	236.3311
7-8	-785.9016	-4963.6	157.8981
8-9	-275.9637	-1742.9	55.4447
9-10	275.9637	1742.9	-55.4447
10-11	785.9016	4963.6	-157.8981
11-12	1176.2845	7429.2	-236.3311
12-13	1235.7786	7805	-248.2843
13-14	1235.7786	7805	-248.2843
14-15	1176.2845	7429.2	-236.3311
15-16	785.9016	4963.6	-157.8981
16-1	275.9637	1742.9	-55.4447

Table 10: Bending Stress for the three Scenarios

Panel	σ Max Climb (psi)	σ Critical Load (psi)	σ Landed (psi)
1	0.15785	0.63607	0
2	0.14584	0.58768	0
3	0.11165	0.4499	0
4	0.060402	0.2434	0
5	2.87E-11	1.15E-10	0
6	-0.060402	-0.2434	0
7	-0.11165	-0.4499	0
8	-0.14584	-0.58768	0
9	-0.15785	-0.63607	0
10	-0.14584	-0.58768	0
11	-0.11165	-0.4499	0
12	-0.060402	-0.2434	0
13	2.87E-11	1.15E-10	0
14	0.060402	0.2434	0
15	0.11165	0.4499	0
16	0.14584	0.58768	0

Authors: z5476963, z5479486, 5479091, z5481625, z5479578, z5676697

Finite element analysis in SolidWorks was performed to generate a general visualization of bending stress concentration in the fuselage. A 3 dimensional model of the idealized fuselage was designed, then an external force was applied to simulate the specified bending load for the maximum climb scenario. The lighter green colored areas of the fuselage represent where bending stress is the highest; these areas correlate with the locations of the booms in the fuselage analysis that had the highest bending stress magnitude.

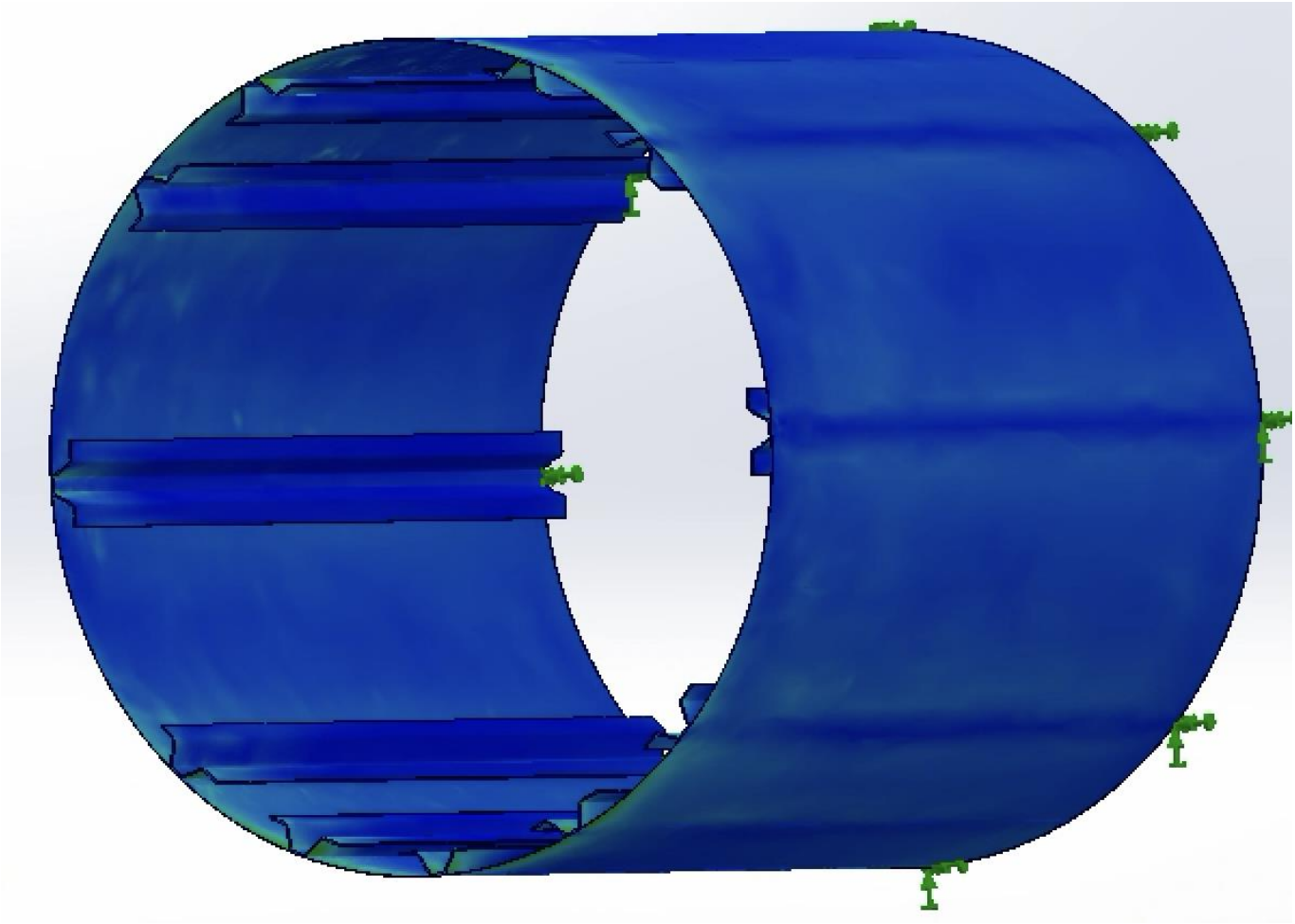

Figure 47 - Fuselage Bending Stress Concentration Plot

7 Allowables and Margins of Safety

7.1 Buckling and crippling allowables – method

Compression failures to an extent can be classed as either non catastrophic or catastrophic. Catastrophic compression failures include global/stiffener column buckling as well as stiffener crippling. These will result in complete structural failure (complete loss of ability to support loads) and thus loss of the aircraft. Non catastrophic failures include less serious buckling modes such as skin local and shear, local stiffener and inter rivet buckling (latter excluded due to a lack of rivet information) which result in non-permanent deformation as well as the not completely compromising the structure's ability to take loads. The loads and stresses at which any of these occur would be equivalent to the allowables of the structure albeit with no room for error.

7.1.1 MATLAB Function Calculations

To obtain the stresses/loads at which buckling/crippling will occur a MATLAB program was used that determined these stresses from rectangular approximations of the shapes of the stiffener and skin, length of the section under analysis, material and boundary conditions of the skin. The program provides two functions one to find catastrophic cases and the other non-catastrophic.

A commonality to both the functions is that they take in rectangular approximations for stiffeners in the form of a line between two points (with x || to the skin and y ⊥ to the skin) with some thickness. This loses some accuracy in the geometry but facilitates the automated determination of free edges as well as various other calculations especially in relation to crippling. Skins are entered in as a thickness and width which is used if relevant. Material is assumed to be the same between fastener and skin. It is taken in as its normal name and the program finds the relevant properties as long as it has been catalogued. It should also be noted that the compressive Young's modulus was assumed to be identical to its tensile variant which results in some disparity but not enough to be of particular concern. This can be changed freely in the material catalogue if such values are determined.

Starting off with the "Catastrophic" cases which regard stiffener column buckling and stiffener crippling a singular function (called "cat") was created to determine both. Stiffener column buckling was chosen as it is a precursor to global buckling and is far easier to analyse as the skin can be assumed to be flat since, as well as another reason, its only for a small section of wing.

To determine the stiffener column buckling load the function looks at a section of the skin stiffener arrangement and assumes the skin has buckled giving it an effective length of 30 thicknesses.

Stiffener column buckling follows the normal equation for column buckling which follows,

$$P_{cr} = \frac{\pi^2 I_{xx} E}{l_e^2}.$$

To get the centroid and some other useful values the points representing the start and end point of the stiffeners are converted to panel widths by Pythagoras theorem. The area of each stiffener panel is then determined to be the width multiplied by a panel's respective thicknesses. The centroid of each stiffener can then be found as an average of the start and end points position. From that the centroid of the entire shape can be found through trivial means.

To get the second moment of area a line integral was taken for each stiffener about the centroid of the entire stiffener and generalised for all cases with an added component for the skin's contribution, both of these utilise a thin wall approximation to make calculations easier and more automatic. This entire

process can be described by the following equation noting I_{yy} is unneeded due to skin being the x axis (column buckling occurs about this axis),

$$I_{xx} = 30t_{skin}\bar{y}_{skin} + \sum_{i}^{stiff} t_i \left[\frac{d_i^3}{3}\sin(\theta_i)^2 + d_i^2(\bar{y}_i)\sin(\theta_i) + d_i{\bar{y}_i}^2\right].$$

The effective length is obtained from the skin width a as it approximately determines the distances between the loaded edges (fuselage frames, wing ribs, etc) and E is obtained by the program after checking what material was specified, past that it is simple substitution to get the load that causes stiffener column buckling.

However, a stress form is more useful as most margins of safety calculations utilise that to get that we can use the function for pressure,

$$\sigma_{cr} = \frac{P_{cr}}{A_{eff}}.$$

Evaluating this is as simple as determining the effective area (take the effective length of the skin into account + stiffener area).

To determine the crippling stress the following value needs to be found for every corner in the stiffener,

$$\sigma_{cc} = \min\left(\sigma_{yield}, c_e\sqrt{\sigma_{yield}E}\left(\frac{b^*}{t^*}\right)^{-\frac{3}{4}}\right).$$

Since this needed to be evaluated at every corner the program would using another custom function (called "connected_edge_list") using a lot of Boolean logic maths determine corners, how many corners, what panels were connected to each corner and if they were free edges.

In a light overview this function worked by finding how many start and end points for the stiffeners were unique, finding how many times each point was repeated, use that to determine how many edges of the stiffener panel were connected (if its not connected there would only be one point in the entire geometry for some unique entry) thus giving a value for if it is free or not, as well as if it was a corner (more than one point in the geometry), count the number of corners.

It should be noted that there is a critical flaw with this method in that the program is actually determining the intersections of stiffeners and not corners. In the case of a stiffener that is created from a flat plate to create shapes such as a hat stringer, w, c or v this would pose no issue as the corners are equivalent to the intersections. However, if it was a more complex shape such as an I, Y or T this would not hold as the corners are defined as stiffeners that form a corner shape. Given the later would be ludicrously hard to do computationally and a quick inspection of various stiffeners reveals they do not show up in the structure a concession would have to be made where any of these more complicated stiffeners would not be possible for the function to find their crippling stresses.

The formula requires some other values for each corner, that is t^* the sum of all the thicknesses of the stiffener panels connected to the corner, b^* the sum of their widths but halved if it is connected between two corners and is c_e which is dependent on material and the number of free edges. The first operation is trivial but the next operation can be done simply by individually dividing relevant stiffener widths by the number of connected edges (how many edges of the panel are connected) and summing. The last operation can be done by referencing a list of c values and utilising a sum of the free edges of all connected stiffener panels. All the material properties are already provided by the material inputted into the function. After evaluating for each corner, it then needs to be turned into an effective for the whole stiffener by,

$$\sigma = \frac{\sum \sigma_{cc} A_c}{\sum A_c}.$$

This is extremely simple to do as A_c is just the area of each corner with its stiffener widths accounting for the halving requirement where needed. The column buckling load and crippling stress are then outputted by the function for manual comparison and analysis against relevant experienced stresses.

For the non-catastrophic case which regards local skin, local stiffener and skin shear buckling a singular function (called "non_cat") once again was able to determine the relevant stresses for all of them.
Both the skin local and shear buckling make use of the aspect ratio of the skin panel, which is simply calculated by,

$$r = \frac{a}{b}.$$

Material properties such as Young's modulus E (tensile assumed to be equivalent to compressive) and Poisson's ratio v are found by the program depending on the entered material.
The stress required to initiate skin local buckling follows,

$$\sigma_{crit} = \frac{k\pi^2 E_c}{12(1-v^2)}\left(\frac{t}{b}\right)^2.$$

The k value is dependent on the boundary conditions of the skin which is an input into the function. k is assumed to be the asymptotic value as the aspect ratio of the skin panels to be analysed is generally very high and k approaches an asymptote as $r \to \infty$. Thus, the program takes a value for k from a list of various values for different boundary conditions without the need for any complex formula or calculation.

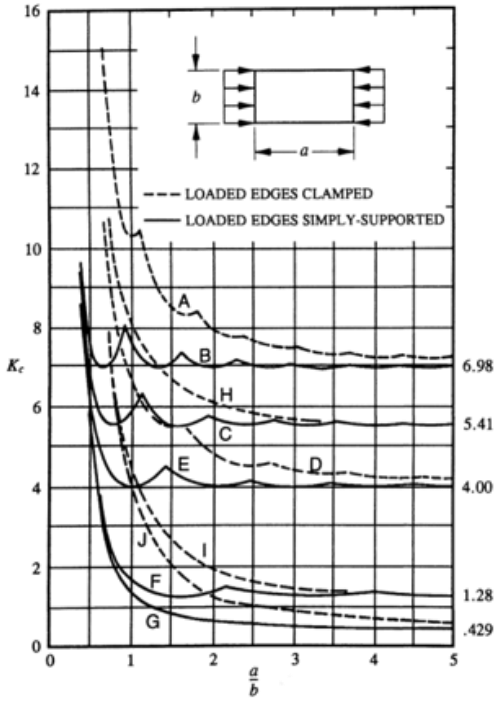

Figure 48 K values for varying boundary conditions

From there a substitution can be made to evaluate the stress to initiate local skin buckling.
The shear stress required to initiate shear buckling in the skin panel is,

$$\tau_{crit} = \frac{\pi^2 K_s E_c}{12(1-v^2)}\left(\frac{t}{b}\right)^2.$$

Similarly to earlier the K_s values are assumed to come from a list of those values for certain boundary conditions since the aspect ratios of the skin panels are large enough that the K_s values would be toward their asymptotes.

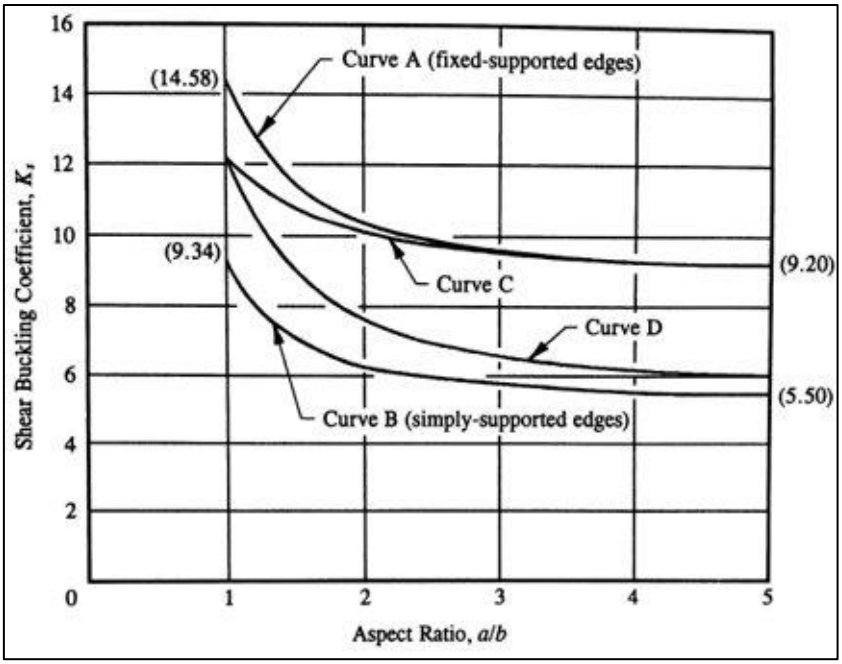

Figure 49 Shear buckling K coefficients

All the other values are identical to the earlier calculation for local skin buckling. Since the function does both at the same time MATLAB just reuses those values.

Thus, the shear stress to initiate shear buckling can be determined by substituting all these values into the equation.

Stiffener local buckling is the result of some panel in the stiffener buckling. This is modelled by splitting all off the stiffener panels up and then evaluating their individual panel buckling stresses which follows,

$$\sigma_{crit\ i} = \frac{k_i \pi^2 E}{12(1-v^2)} \left(\frac{t_i}{b_i}\right)^2 .$$

The width of each stiffener can be calculated through Pythagoras theorem on their start and end points. Thickness is already provided, and material properties follow that specified by the inputs as mentioned previously.

For this case k can be assumed to be the asymptotic values ($r \to \infty$) from Figure 48. This is because the stiffeners have an extremely high aspect ratio owing to it being thin and running along entire sections of the aircraft.

From there the k values specific to some boundary condition following how the individual stiffener panel makes up the stiffener. Specifically, the "Loaded edges" are the ends of the stiffener and are assumed to be simply supported, the other two edges are clamped or free depending on if it joins to other panels in the stiffener or isn't respectively. The program determines this boundary condition using the number of connections to either edge of each stiffener, which was obtained from the same custom function used previously for the crippling calculations.

Through a simple substitution the individual panel buckling stress of each stiffener panel can be found. From there the minimum is taken as it would be the stress that will induce local stiffener buckling somewhere in the stiffener.

7.1.2 Usage Notes

It should be recognised that this function determines different critical loads and stresses for flat stiffener skin arrangements at the same time. Despite that it is possible to use it to generate values for just a skin panel or just a stiffener on some thickness skin. This can be done by ignoring relevant values such as if it is just a skin panel any of the values that utilise the stiffener such as crippling, stiffener column and local buckling can be ignored (they would not have been evaluated if this was done manually as they simply do not apply). "Skin" is also more correctly a panel so something such as a spar or plate can be determined with the program.

Some notable case for this slight deviation would be the wing spars as well as the small panel covering the gap between the wing and the aileron where in both cases there is no stiffener (so only values relating to just "skin" should be taken).

It should also be noted that stiffener column buckling is the only calculation to utilise geometry for both the stiffener and skin yet since it only utilises the skin thickness it would be valid regardless of the size of the skin panel. This means its on the geometry a boom panel analysis if all the skin is the same stiffness evaluating the stiffener column buckling for one boom would give a value for the entire geometry.

For the readers interest the reason the functions evaluate all the values at once is an initially flawed understanding of how many cases (skin panel bounding conditions) there would be.

7.2 Material allowables (yielding) – Method

The point a material yields can vary depending on how it is loaded. Through the von mises yield criterion a combination of stresses in principle axis to cause yielding can be found in 2D by the equation,

$$\sigma_y^2 = \sigma_1^2 - \sigma_1\sigma_2 + \sigma_2^2.$$

The entire structure has been assumed to consist of aluminium 2024-T3 which has a yield stress of $50kips$. So, the combination of normal stresses on the material must follow,

$$2500 > \sigma_1^2 - \sigma_1\sigma_2 + \sigma_2^2.$$

The principal stresses for some combination of normal stresses and shear stresses for an arbitrary axis can be found to be,

$$\sigma_1 = \frac{\sigma_x + \sigma_y}{2} + \sqrt{\left(\frac{\sigma_x - \sigma_y}{2}\right)^2 + \left(\tau_{xy}\right)^2}, \quad \sigma_2 = \frac{\sigma_x + \sigma_y}{2} - \sqrt{\left(\frac{\sigma_x - \sigma_y}{2}\right)^2 + \left(\tau_{xy}\right)^2}.$$

This can then be determined for every combination of stresses and checked against the von mises criteria shown earlier to determine if material failure has occurred.

7.3 Fatigue

Fatigue is an important part of structural analysis as it provides insight into how safe it is to continue operation after a determined amount of time or cycles. Fatigue occurs as a result of repeated stresses upon the structural elements of the aircraft, which over time can cause a significant decline in safety for the pilot, passengers and the environment. For the Piper Archer specifically, the aircraft is mainly used for training or recreational purposes meaning that each owner is likely to fly and treat their aircraft differently. Training aircraft are used in a very cyclical manner since trainee pilots must complete their hours and develop proficiency in set manoeuvres as opposed to recreational usage which is almost random. Due to this, the following analysis will focus on the cyclical flights done by the Piper Archer in a training context. Over an average of 10 flights the frequency of some general manoeuvres has been tabulated in Table 11.

Table 11: Frequency of standard manoeuvres over ten flights.

Manoeuvre	Frequency (Over 10 Flights)
Take Off	10
Landing	10
Climbing	40
Descent	40
Turn	100
Steep Turn	10
Stall / Recovery	5
Glide	5
Slow Cruise (close to stall speed)	10
Cruise	20

To graph the stresses each manoeuvre places upon the airframe, experimental data would be required using strain gauges mounted along the wing spars and fuselage. As this is not available to us at this time, the manoeuvres were sorted into either high fatigue or low fatigue and displayed in Table 12 as percentages of total manoeuvres.

Table 12: Categorisation of Manoeuvres based on Fatigue

Manoeuvre	Fatigue Category	Frequency (Over 10 Flights, %)
Take Off	High	4%
Landing	High	4%
Climbing	Low	16%
Descent	Low	16%
Turn	Low	40%
Steep Turn	High	4%
Stall / Recovery	High	2%
Glide	Low	2%
Slow Cruise (close to stall speed)	Low	4%
Cruise	Low	8%

From the assumptions, the aircraft spends much of its life in low fatigue (based on stress) manoeuvres, approximately 86%, with the remaining 14% being in high fatigue situations. Since, again the exact loadings for each manoeuvre are unable to be calculated without experimental data, the low fatigue case will be analysed based on the stresses observed by the aircraft in cruise and the high fatigue case will be modelled by the maximum climb data already available in section 6, Analysis of this report. The maximum shear and bending stresses on the wing and fuselage for the maximum climb case from section 6 Analysis, have been extracted into Table 13: Maximum stresses from Maximum Climb and Cruise casesTable 13. Using the same method, maximum stresses for the cruise case were calculated.

Table 13: Maximum stresses from Maximum Climb and Cruise cases ($\boldsymbol{Imperial}$)

	Maximum Climb		Cruise	
	Shear Stress ($\boldsymbol{psi}$)	**Bending Stress ($\boldsymbol{psi}$)**	**Shear Stress ($\boldsymbol{psi}$)**	**Bending Stress ($\boldsymbol{psi}$)**
Wing	-4595.036	-1437.21	-3805.28	-899.84
Fuselage	1235.7786	0.15785	367.235	0.0213

The stress values can be compared with an average lifespan using an alternating stress, S-N curve. These plots are typically in mega pascals and only the absolute values are required as the stress is alternating. As such, the values must be converted as shown in Table 14

Table 14: Maximum stresses from Maximum Climb and Cruise cases ($\boldsymbol{Metric}$)

	Maximum Climb		Cruise	
	Shear Stress ($\boldsymbol{MPa}$)	**Bending Stress (MP$\boldsymbol{a}$)**	**Shear Stress ($\boldsymbol{MPa}$)**	**Bending Stress (MP$\boldsymbol{a}$)**
Wing	31.68	9.90	26.23	6.20
Fuselage	8.52	0.001088	2.53	0.00014

The stress to number of cycles (S-N) plot varies for each material. In Section Material Properties, the aerostructure was shown to be made of Aluminium alloys, particularly Al 2024-T3. An appropriate plot has been sourced from the AERO3410 MATLAB directory, can be sources from section 9, ‘

Authors: z5476963, z5479486, 5479091, z5481625, z5479578, z5676697

Directory of Supplementary Information' and is shown in Figure 50.

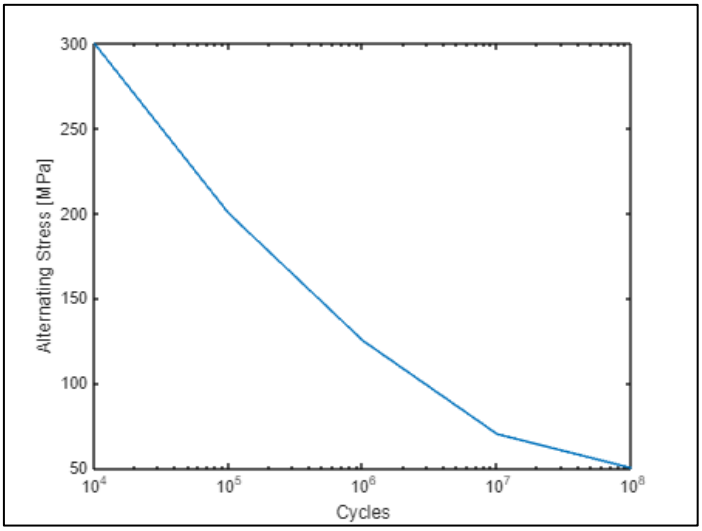

Figure 50: Aluminium S-N plot - AERO3410 MATLAB directory

The lifetime for a singular alternating stress can be found simply through linear interpolation of this lot at a given stress. The maximum stress of 31.68 MPa acting on part of the wing during maximum climb is not visible on the plot, meaning it is under the endurance limit and will cause negligible fatigue.
However, when multiple stresses act concurrently, it is more likely that that fatigue will be caused to a component. To estimate the lifetime in this situation, 'Miner's Theorem' can be used. This theorem states that a component will fail when the sum of the life fractions equals 1, where a life fraction is a particular stress's individual contribution to the total fatigue. Mathematically this is,

$$\frac{n_1}{N_1} + \frac{n_2}{N_2} + \cdots + \frac{n_n}{N_n} = 1$$

Using the MATLAB code (from aforementioned directory), the result is still showing that the fatigue is negligible. This can be expected, as the aircraft is manufactured under rigorous standards and when flown under the recommended conditions should last almost indefinitely.
It is likely that stress concentrations may make themselves present at various points of the airframe. These tend to appear anywhere where there is a irregularity in the surface geometry, for example within holes, notches, fillets and potentially from any damage the skin may have endured during flight or taxi. The damage itself does not always present an immediate issue, but as the discontinuity prevents even flow of stress, the concentration can be up to 5 times the expected amount, this can be a problem. Figure 51 is an S-N plot for Al2024-T3, and shows four lines, each modelling the impact of a degree of stress concentration.

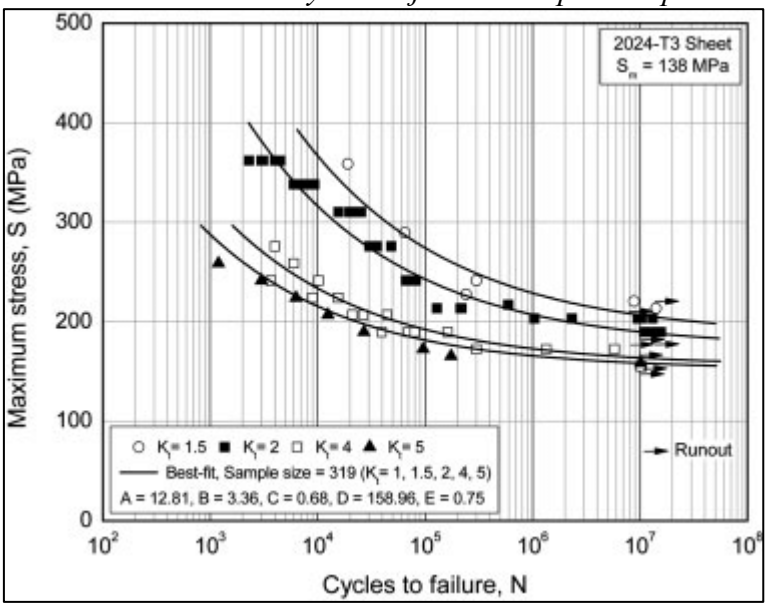

Figure 51: S-N Plot showing Stress concentration factors (K) (Kassim S, 2008)

Examining the values at 10^5 cycles, Table 1has been produced

Table 15: Maximum stresses to extend lifetime to 10^5 cycles at varying concentration factors.

Stress Concentration Factor (K)	Approx. Maximum Stress (MPa) for $N = 10^5$
1.5	280
2	250
4	190
5	180

The table shows that for a component to last for a set number of cycles ($N = 10^5$), the presence of a stress concentration greatly reduces that maximum stress it can withstand. A concentration of $K = 1.5$ is $100MPa$ less that a concentration $K = 5$. The earlier analysis had shown that with correct usage there would be no fatigue on the wing, however if a stress concentration of $K = 4$ were to form the shear stress on the wing during maximum lift could be

$$S = 31.68 \times K$$
$$= 126.72\ MPa$$

This value certainly does appear on the initial SN plot and through linear interpolation would cause fatigue towards failure after $N = 9.5 \times 10^5$ cycles. Following this, a scatter factor of 2 can be applied to ensure safety, further minimising this lifespan to $N = 4.75 \times 10^5$ cycles. This value is still large, but it is no longer negligible. Similar results should be expected for the other stresses present on the wing and fuselage should they encounter stress concentration.

7.4 Margins of safety – Fuselage

From section 6.3 the fuselage was simplified to be a perfect cylinder of 21.683" radius with 16 equidistant booms every 8.504" of its perimeter (Figure 46). All booms were stiffeners except for booms 4,6,12,14. Skin thickness was found to be 0.032". Due to the nature of the divisions the panels slight curvature will be approximated to be flat resulting in only a marginal error in a smaller loads and stresses and thus MS. This is done in order to make calculations easier (no need to account for curvature parameter or extra complexity) and work with the MATLAB functions explained previously.

The actual geometry of the stiffeners is unknown but from the manual it is possibly an inverted hat due to the apparent shape of the stringers in the parts manual and the aircraft appearing to have a single row of rivets to attach each stringer to the fuselage. A possible option for the stiffener geometry is as follows,

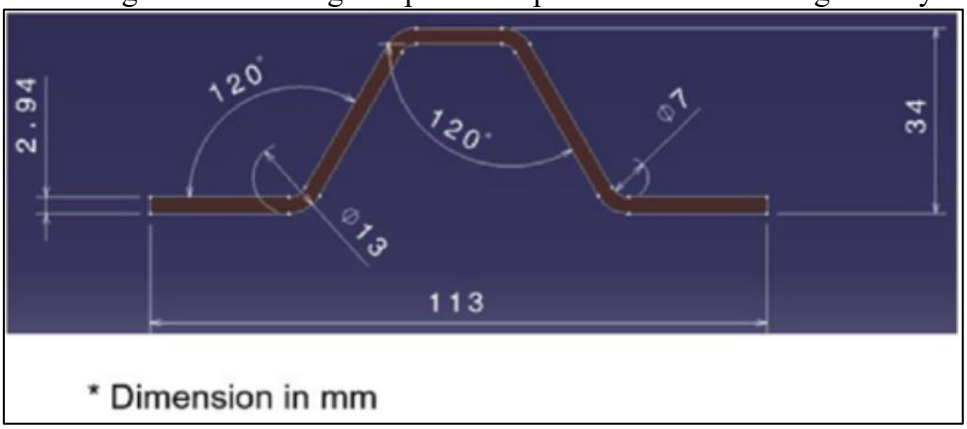

Figure 52 Possible stiffener option

The lack of geometry for the flat sections means an assumption has to be made. This assumption will be that they are all equally long. It will also be wise to approximate the entire stiffener as just thin-walled panels and exclude the rounded sections as they are effectively just a sharp corner.

Through some simple geometry this results in a stiffener approximated (in imperial units) as follows:

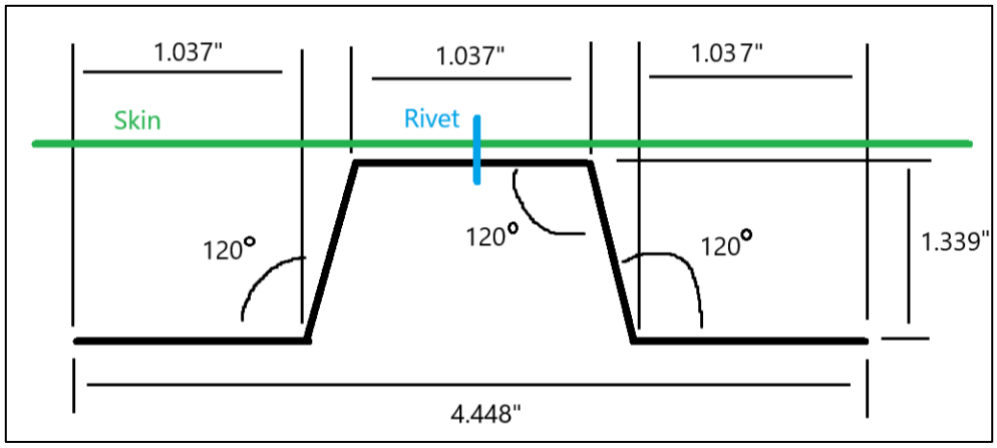

Figure 53: Simplified Stiffener Geometry (not to scale)

The fuselage is roughly half the length of the total tip to tail length giving a length of 126”. It is assumed that a single skin panel spans this length between booms/stiffeners with only constraints on its boundary. Such a boundary is presumed to be clamped loaded edges (connections to fuselage frame) and all else simply supported (due to inverted hat stiffener) on both sided.

Due to the panels between 3-5, 5-6, 11-13 and 13-15 having a boom without a stiffener, to conduct the buckling crippling analysis they will need to be considered as a different size skin panel to the others. Due to the interactions of the various calculations this will only result in differences in skin local and shear buckling needing to be determined individually and the shear stress over each being averaged.

Table 16: Catastrophic and Non-Catastrophic allowable load/stress values for Fuselage

	Catastrophic	Non-Catastrophic

	Stiffener column buckling (psi)	Stiffener Crippling (kips)	Skin local buckling (psi)	Skin Shear Buckling (psi)	Stiffener local buckling (kips)
8.504" panels	1985	49.922	581.84	831.19	156.00
17.008" panels			145.46	207.80	

The margin of safety is calculated by,

$$MS = \frac{allowable}{applied} - 1.$$

Normal stresses on a panel are roughly equivalent to the average stresses experienced by the connected booms.

Looking at the maximum normal and shear stresses experienced by any panel under critical loading and calculating the MS gives numerous values presented here.

Table 17: Margins of safety for different geometry panels and failure modes for fuselage

	Stresses		Catastrophic		Non-Catastrophic		
	Normal Stress (psi)	Shear Stress (psi)	Stiffener column buckling MS	Stiffener Crippling MS	Skin local buckling MS	Skin Shear Buckling MS	Stiffener local buckling MS
8.504" panels	0.611875	4963.6	3243.127	81587.56	949.9132	-0.83254	254953
17.008" panels	0.63607	78484	3119.726	78484.07	227.6855	-0.97272	245255

Consider under ultimate loading conditions non-catastrophic allowables likely would have been surpassed and catastrophic should be about to be surpassed giving a negative and a small positive MS respectively. This surprisingly does not appear to be the case with the only failure occurring being the skin due to shear buckling. There is also a very high MS for other worse of panels. This is somewhat sensible due to the normal stress values being effectively 0 which would result in the extremely high MS values for any failure mode dependent on normal stresses. Skin shear buckling also appears to occur on the aircraft with images of the aircraft in flight appearing to have warping along its surface.

When it comes to yield the stresses experienced by the structure is symmetric both vertically and horizontally. So, evaluating the margins of safety in relation to yield for the top quarter of panels clockwise gives.

Table 18 Material Yield margins of safety for fuselage

Panel	Shear (psi)	Normal stress on panel (psi)	C (psi)	R (psi)	p1 (psi)	p2 (psi)	von	MS
01	0.63607	0.611875	0.305938	1742.9	1743.206	-1742.59	3018.792	15.56292
02	0.58768	0.51879	0.259395	4963.6	4963.859	-4963.34	8597.207	4.815842
03	0.4499	0.34665	0.173325	7429.2	7429.373	-7429.03	12867.75	2.885683
04	0.2434	0.1217	0.06085	7805	7805.061	-7804.94	13518.66	2.698592

It appears that the material yield margins of safety are still completely fine despite the critical loading conditions. This is very much expected as it is well known that generally for semi monocoque structures failure generally occurs in the form of buckling or crippling far before the material limits are reached.

7.5 Margins of safety – Wing

From earlier (p.g.27) the wing box was analysed through a boom panel analysis as a 24-boom structure with constant thickness panels of 0.025in. The booms in the wing section were based upon stiffener positions.

The actual geometry of the stiffeners are unknown but are possibly the same hat fastener from earlier due to the apparent shape of the stringers in the parts manual and the aircraft appearing to have a double row of rivets to attach each stringer along the wing. The hat fastener means that every panel except for 01-02 and 23-24 can be modelled with a fully clamped edge boundary conditions which makes life a lot easier.

Due to the exceptional difficulty in evaluating values due to the wings taper, the wing will be assumed to be rectangular and empty with ribs only at the start and ends of the wing (so skin panel length a = 189.32”). All other geometry will follow that in section 6.1.

The sheer quantity of panels to analyse calls for a modification to the MATLAB program to go through every panel and obtain a value for them.

Modifying the code to conduct a calculation at every single panel and boom in order to generate numerous margins of safety for every panel and boom accounting for the relevancy of certain results gives the following tables.

Table 19 Skin local, shear and yielding margins of safety calculations

Panel	Skin local buckling (psi)	Skin shear Buckling (psi)	Normal stress in panel (psi)	Shear stress in panel (psi)	Margin safety skin local bucklin g	Margin safety shear bucklin g	Principle stress 1	Principle stress 2	Von mises result	Margin of safety from yieldin g
"01-02"	8439.58	10783.91	8427.32	-4229.52	0.00	1.55	10183.90	-1756.58	11166.30	3.48
"02-03"	2344.86	2996.21	7616.18	18015.00	-0.69	-0.83	22221.18	-14605.00	32118.95	0.56
"03-04"	1006.77	1286.43	5954.40	12232.12	-0.83	-0.89	15566.42	-9612.02	22007.48	1.27
"04-05"	1006.77	1286.43	3189.70	6016.88	-0.68	-0.79	7819.51	-4629.81	10898.75	3.59
"05-06"	3672.28	4692.36	838.03	367.98	3.38	11.75	976.67	-138.64	1052.86	46.49
"06-07"	461.91	590.22	2271.98	14505.96	-0.80	-0.96	15686.36	-13414.39	25227.57	0.98
"07-08"	1006.41	1285.97	5788.61	8400.96	-0.83	-0.85	11779.86	-5991.25	15660.02	2.19
"08-09"	5158.07	6590.87	7351.13	3548.24	-0.30	0.86	8784.35	-1433.23	9581.70	4.22
"09-10"	3225.50	4121.47	8186.33	-1093.21	-0.61	2.77	8329.80	-143.47	8402.45	4.95
"10-11"	1004.66	1283.74	8799.45	-5982.24	-0.89	-0.79	11825.67	-3026.23	13593.82	2.68
"11-12"	629.95	804.94	6956.21	-9937.68	-0.91	-0.92	14006.86	-7050.65	18565.05	1.69
"12-13"	16123.72	20602.53	0.00	-11207.20	Inf	0.84	11207.20	-11207.20	19411.44	1.58
"13-14"	629.95	804.94	-6956.21	-10663.36	-0.91	-0.92	7738.16	-14694.36	19736.02	1.53
"14-15"	1004.66	1283.74	-8799.45	-8742.88	-0.89	-0.85	5387.80	-14187.24	17514.11	1.85
"15-16"	3225.50	4121.47	-8186.33	-5680.68	-0.61	-0.27	2908.56	-11094.88	12799.46	2.91
"16-17"	5158.07	6590.87	-7351.13	-2319.39	-0.30	1.84	670.62	-8021.75	8377.21	4.97
"17-18"	1006.41	1285.97	-5788.61	489.92	-0.83	1.62	41.17	-5829.78	5850.47	7.55
"18-19"	461.91	590.22	-2271.98	2807.65	-0.80	-0.79	1892.77	-4164.75	5367.55	8.32
"19-20"	3672.28	4692.36	-838.03	-14511.08	3.38	-0.68	14098.12	-14936.14	25147.89	0.99
"20-21"	1006.77	1286.43	-3189.70	-11299.20	-0.68	-0.89	9816.35	-13006.05	19829.02	1.52
"21-22"	1006.43	1286.00	-5954.40	-8187.24	-0.83	-0.84	5734.55	-11688.95	15380.10	2.25
"22-23"	2344.86	2996.21	-7616.18	-4825.48	-0.69	-0.38	2339.01	-9955.19	11307.61	3.42
"23-24"	8439.58	10783.91	-8427.31	-28435.48	0.00	-0.62	24532.32	-32959.64	49967.48	0.00
"02-23"	4770.82	6096.05	0.00	-26933.44	inf	-0.77	26933.44	-26933.44	46650.09	0.07
"06-19"	2975.70	3802.28	0.00	-21271.80	Inf	-0.82	21271.80	-21271.80	36843.84	0.36

Table 20 Stiffener column buckling, crippling and local buckling margins of safety and calculations

Boom	Stiffener column buckling (psi)	Stiffener crippling (psi)	Stiffener local buckling (psi)	Margin of safety Stiffener column Buckling	Margin of safety stiffener crippling	Margin of safety stiffener local buckling
"01"	843.78	49922.37	155997.39	-0.90	4.66	16.67
"02"	843.78	49922.37	155997.39	-0.89	5.22	18.43
"03"	843.78	49922.37	155997.39	-0.88	5.93	20.65
"04"	843.78	49922.37	155997.39	-0.82	9.61	32.17
"05"	843.78	49922.37	155997.39	-0.50	28.79	92.07
"06"	843.78	49922.37	155997.39	Inf	Inf	Inf
"07"	843.78	49922.37	155997.39	-0.81	9.99	33.33
"08"	843.78	49922.37	155997.39	-0.88	6.10	21.18
"09"	843.78	49922.37	155997.39	-0.89	5.51	19.34
"10"	843.78	49922.37	155997.39	-0.90	4.74	16.92
"11"	843.78	49922.37	155997.39	-0.91	4.61	16.54
"12"	843.78	49922.37	155997.39	-0.83	8.95	30.09
"13"	843.78	49922.37	155997.39	-0.83	8.95	30.09
"14"	843.78	49922.37	155997.39	-0.91	4.61	16.54
"15"	843.78	49922.37	155997.39	-0.90	4.74	16.92
"16"	843.78	49922.37	155997.39	-0.89	5.51	19.34
"17"	843.78	49922.37	155997.39	-0.88	6.10	21.18
"18"	843.78	49922.37	155997.39	-0.81	9.99	33.33
"19"	843.78	49922.37	155997.39	Inf	Inf	Inf
"20"	843.78	49922.37	155997.39	-0.50	28.79	92.07
"21"	843.78	49922.37	155997.39	-0.82	9.61	32.17
"22"	843.78	49922.37	155997.39	-0.88	5.93	20.65
"23"	843.78	49922.37	155997.39	-0.89	5.22	18.43
"24"	843.78	49922.37	155997.39	-0.90	4.66	16.67

The margins of safety for the individual panels reveals that the wing would have failed quite badly with stiffener column buckling occurring for every stiffener. Given that is a catastrophic failure the aircraft would not have survived the critical load case.

8 Conclusions and Limitations

The investigation set out to determine the extent of fatigue evident on a Piper Archer II that is utilised as a training aircraft. It was expected that an aircraft that maintains regular maintenance for deformations or associated damage will be able to operate almost indefinitely from a structural point of view. Fatigue analysis alongside a determination of margins of safety were conducted on a simplified model of the aircraft to ascertain that this was inherently true. However, due to the necessary assumptions and simplifications in both the establishment of structural geometry and calculation methods, an element of inaccuracy and error is likely prevalent.

Limitations from the VSPAERO analysis arise from the use of the Vortex-Lattice Method to solve for inviscid potential flow. The method doesn't take into consideration the viscous boundary layer flow, and as such viscous effects such as parasitic drag are estimated in software using empirical corrections based on the airfoil and flow parameters. This limits the accuracy of the drag calculations, which in turn decreases the accuracy of the stress analysis in the x direction of the aircraft. Further limitations in the horizontal stabiliser analysis specifically came from the estimation of elevator deflection angle. Elevator trim is dependent on the weight distribution in the aircraft and so changes flight to flight. Finally, due to the shorter span of the stabiliser and inherent noise in the drag calculation in the Vortex-Lattice Method, the data for CD needed to be smoothed in MATLAB to show meaningful curves but introducing error.

Another limitation arose from estimating the stress in the wing, the geometry was first idealised with the boom points and spar locations. The geometry, specifically for the Piper Archer II was not found, and the sketch was made from the readings of tests from other similar aircrafts. The assumptions made here include the actual shape of the wing box, coordinates of the boom points, and the area of the stiffener. Another assumption made for the simplification of the calculations was that the skin thickness and the chord length is constant throughout the wing. These values are not constant, but the variation of them is similar, hence this assumption was made.

The fatigue analysis showed clearly that under the expected use cases, the aircraft and structure experiences alternating stresses well under the endurance limit of its primary material Al2024-T3 and as a result, will not fatigue by any noticeable amount. However, through the application of a scatter factor and in the presence of a stress concentration, the components to find themselves on the S-N curve, however the lifespan does continue to be very long, approximating to be within a magnitude of 10^5 cycles.

The analysis of the margins of safety for buckling, crippling and material yielding revealed that the fuselage of the aircraft is stunningly resistant to loading only suffering non catastrophic structural failure in skin buckling which given the functionality of that specific part of the fuselage would pose no risk. Unfortunately, the wings are not nearly as resilient with them suffering negative margins of safety close to -1 especially in relation to column buckling. A likely reason for this is not that the aircraft is horrifically unfit for flight but that the geometry estimations were incorrect. The most likely culprit being the length of the skin panels on the wings. A lack of information on wing rib position meant an assumption that the skin covers the entire wing without one was made. This would greatly reduce the calculated values to induce buckling from their true value. In retrospect obtaining the correct rib positioning would be vital to obtaining a more accurate value.

9 References

A. (n.d.). Retrieved from A.

Al-Shamma, O., & Ali, R. (2014). AIRCRAFT WEIGHT ESTIMATION IN INTERACTIVE DESIGN PROCESS.

Kassim S, A.-R. (2008, June). *General Model for Stress-life fatigue prediction.* Retrieved from ResearchGate: https://www.researchgate.net/figure/S-N-curves-for-2024-T3-aluminium-alloy-large-sample-of-fatigue-data-S-m-138-MPa-Abb_fig3_247989167

NASA STI Program Office. (2001, March). *AST Composite Wing.* Retrieved from https://ntrs.nasa.gov/api/citations/20010033249/downloads/20010033249.pdf

PILOT'S OPERATING HANDBOOK. (1975, August 15). Retrieved from PIPER CHEROKEE ARCHER II: https://stpeteair.org/wp-content/uploads/PA-28-181-Archer-II-POH-.pdf

Piper Aircraft Corporation. (1975, August 15). *PIPER CHEROKEE ARCHER II*. Retrieved from PILOT'S OPERATING HANDBOOK: https://stpeteair.org/wp-content/uploads/PA-28-181-Archer-II-POH-.pdf

Piper Aircraft Corporation. (1994, July 30). Airplane Maintenance Manual. Florida, U.S.A.: Technical Publications.

Piper Aircraft Corporation. (1994, September 15). Airplane Parts Catalog. Florida, U.S.A.: Technical Publications.

Piper Aircraft Corporation. (n.d.). Piper Archer II Performance and Specifications.

Piper Aircraft Corporations. (1975, August 15). *PIPER CHEROKEE ARCHER II*. Retrieved from PILOT'S OPERATING HANDBOOK: https://stpeteair.org/wp-content/uploads/PA-28-181-Archer-II-POH-.pdf

skytamer.com. (1998). *Piper Cherokee Archer II*. Retrieved from Skytamer Images: https://www.skytamer.com/Piper_PA-28-181.html

10 Directory of Supplementary Information

10.1 Draft Report - Draft Report.docx
Much of the material in this report has been copied across from a draft document titled "Draft Report.docx". In case the document history isn't visible in the submitted .zip file, the original documents can be found under the group's MS Teams channel (Group R).

10.2 Wing Loading MATLAB Code
The MATLAB code for this section is named "Calc_Wing_Loads.m" and is attached in the submitted folder. The code calls upon a .CSV file from VSPAERO, two of which are also attached in the folder. The code is currently set up to work with the critical loading scenario (using "Crit Loading Data.CSV").

10.3 Wing OpenVSP File - Wings.vsp3

10.4 Fuselage Loading MATLAB Code
The MATLAB code for fuselage loading is separated into 3 files for each load case named "Fuselagemax.m," "Fuselagecrit.m," and "Fuselageland.m" and are all are attached in the submitted folder.

10.5 Fatigue Calculation MATLAB Code - Properties_and_Lifetimes_E02_E03.mlx

10.6 Meeting Minutes - Meeting Minutes

10.7 Empennage Loading MATLAB Code - AERO3410Empennage.mlx

10.8 Piper Archer II OpenVSP File (used for empennage) - PiperArcher.vsp3

10.9 **Pilot's Operating Handbook -** Pilots Operating Handbook.pdf

10.10 Maintenance Manual - Maintenance Manual.pdf

10.11 Airplane Parts Catalogue - Airplane Parts Catalog.pdf

10.12 Performance and Specifications - Piper Archer II Performance **(Piper Aircraft Corporation)**and Specifications.pdf

10.13 Buckling Crippling and Yielding margins of safety code
The MATLAB code for this section is aptly named "buckling_for_the_group_task_thing.m" and is in the attached folder. The code is entirely self contained and will determine the Buckling and Crippling loads and stresses for both the fuselage and the wing box utilising all the relevant assumptions and data without additional input. It will also determine the margins of safety for buckling crippling and yielding for the wing box. (Fuselage was done manually)